Bounce Resonance between Energetic Electrons and Magnetosonic Waves: A Parametric Study

Shujie Gu[1] and Lunjin Chen[2]

[1]The University of Texas at Dallas
[2]University of Texas at Dallas

September 11, 2023

Abstract

Magnetosonic waves are electromagnetic emissions from a few to 100 Hz primarily confined near the magnetic equator both inside and outside the plasmasphere.
Previous studies proved that MS waves can transport equatorially mirroring electrons from an equatorial pitch angle of 90° down to lower values by bounce resonance.
But the dependence of bounce resonance effect on wave or background plasma parameters is still unclear.
Here we applied a test particle simulation to investigate electron transport coefficients, including diffusion and advection coefficients in energy and pitch angle, due to bounce resonance with MS waves.
We investigate five wave field parameters, including wave frequency width, wave center frequency, latitudinal distribution width, wave normal angle and root-mean-square of wave magnetic amplitude, and two background parameters, \$L\$-shell value and plasma density.
We find different transport coefficients peaks resulted by different bounce resonance harmonics. Higher order harmonic resonances exist, but the effect of fundamental resonance is much stronger. As the wave center frequency increases, higher order harmonics start to dominate. With wave frequency width increasing, the energy range of effective bounce resonance broadens, but the effect itself weakens.
The bounce resonance effect will increase when we decrease the wave normal angle, or increase the wave amplitude, latitudinal distribution width, L-shell value, and plasma density.
The parametric study will advance our understanding of the favorable conditions of bounce resonance.

Bounce Resonance between Energetic Electrons and Magnetosonic Waves: A Parametric Study

Shujie Gu[1] **and Lunjin Chen**[1]

[1]Department of Physics, W.B. Hanson Center for Space Sciences, University of Texas at Dallas, Richardson, TX, USA

Key Points:

- Higher order harmonic resonances are important with high wave center frequency.
- The bounce resonance effect tends to increase with increasing wave latitudinal width, wave amplitude, L-shell value and background plasma density.
- Increasing wave normal angle and wave frequency width can decrease the bounce resonance effect.

Corresponding author: Shujie Gu, `shujie.gu@utdallas.edu`

Abstract

Magnetosonic waves are electromagnetic emissions from a few to 100 Hz primarily confined near the magnetic equator both inside and outside the plasmasphere. Previous studies proved that MS waves can transport equatorially mirroring electrons from an equatorial pitch angle of 90° down to lower values by bounce resonance. But the dependence of bounce resonance effect on wave or background plasma parameters is still unclear. Here we applied a test particle simulation to investigate electron transport coefficients, including diffusion and advection coefficients in energy and pitch angle, due to bounce resonance with MS waves. We investigate five wave field parameters, including wave frequency width, wave center frequency, latitudinal distribution width, wave normal angle and root-mean-square of wave magnetic amplitude, and two background parameters, L-shell value and plasma density. We find different transport coefficients peaks resulted by different bounce resonance harmonics. Higher order harmonic resonances exist, but the effect of fundamental resonance is much stronger. As the wave center frequency increases, higher order harmonics start to dominate. With wave frequency width increasing, the energy range of effective bounce resonance broadens, but the effect itself weakens. The bounce resonance effect will increase when we decrease the wave normal angle, or increase the wave amplitude, latitudinal distribution width, L-shell value, and plasma density. The parametric study will advance our understanding of the favorable conditions of bounce resonance.

Plain Language Summary

There are various plasma waves and wave-particle interactions in the magnetosphere and they are crucial for magnetosphere dynamics. Bounce resonance between electrons and magnetosonic waves is one of them and plays an essential role in removing equatorially mirroring electrons. Magnetosonic waves are electromagnetic emissions from several Hz to 100 Hz confined near the magnetic equator. The energetic electrons can be scattered by magnetosonic waves by bounce resonance. In this study, we run a test particle simulation and investigate the bounce resonance effective regime. The wave and background parameters are studied, including root-mean-square of wave magnetic amplitude, wave frequency width, center frequency, latitudinal width, wave normal angle, plasma density and$L$-shell value. The parametric study will improve our modeling of radiation belt dynamics.

1 Introduction

Magnetosponic(MS) waves, also called as equatorial noise (Russell et al., 1969) or equatorial MS waves (Ma et al., 2013), are ion Berstein mode waves driven by a proton velocity ring distribution with a positive slope in $\partial f_p(v)/\partial v_{perp}$ (Gary et al., 2010; K. Liu et al., 2011). They are magnetically compressional mode electromagnetic waves excited at very oblique wave normal angles and propagate nearly perpendicular to the background magnetic field (Chen et al., 2011; Chen & Thorne, 2012). Observationally, MS waves generally occur latitudinally near Earth's magnetic equator with a frequency range from the proton gyrofrequency f_{cp}(several Hz) to the lower hybrid frequency f_{LHR}(about 100 Hz) (Gurnett, 1976) and consist of discrete equally spacing spectral lines (Santolík et al., 2004; Min et al., 2018), which are multiples of f_{cp}. They are located both inside and outside the plasmasphere, and recent studies observed their occurrence in very low altitudes at the ionosphere with very strong geomagnetic activities(Hanzelka et al., 2022). The strong MS waves can be measured with the amplitudes of the dominant wave magnetic component around 50 pT for average cases (Ma et al., 2013) and 1 nT for extremely strong cases (Tsurutani et al., 2014).

Bounce resonance between electromagnetic waves and energetic particles have been well studied since Roberts and Schulz (1968) first formulated the theory. Bounce motion plays an important role in accelerating and scattering particles through wave-particle interactions with different waves in the magnetosphere, such as bounce resonance between EMIC waves and electrons with hundreds of keV (e.g. Blum et al., 2019; Cao et al., 2017) and drift-bounce resonance between Pc4-5 ULF waves and ions with tens of keV (e.g. Zhu et al., 2020; Z.-Y. Liu et al., 2020). Previous studies paid much more attention to gyroresonance and drift resonance interaction than bounce resonance. Equatorially mirroring energetic electrons, however, are generally immune to the gyroresonance interaction since it requires a finite parallel velocity along the field line to satisfy the gyroresonance condition when the electrons energies are not large enough to provide a sufficient relativistic Lorentz factor to reduce the gyrofrequency. But the observations have shown that equatorially mirroring electron flux in the radiation belt cannot build up continuously (Shprits, 2009).

To solve this problem, Chen et al. (2015) proposed a loss mechanism of equatorially mirroring electron by nonlinear bounce resonance between MS waves and equatorially mirroring energetic electrons, to account for the transportation of pitch angle from 90° to lower values, which enables the scattering of those electrons out of equatorial plane. The capability of removing equatorially mirroring electrons from 90° due to bounce resonance results in a butterfly distribution, a minimum at 90° in pitch angle distribution, observationally reported by Maldonado et al. (2016). Thus the bounce resonance transport process plays a vital role in electron scattering in radiation belt and the electron flux depletion during geomagnetic storms. The bounce resonance diffusion coefficients have been investigated through quasilinear diffusion theory and their formulas have been developed in a more realistic MS wave model, with the finite Larmor radius effect and Gaussian latitudinal distribution of wave intensity (Roberts & Schulz, 1968; Li et al., 2015; Tao et al., 2016; Li & Tao, 2018; Maldonado & Chen, 2018; Chen & Bortnik, 2020). The derived formulas are targeted for broadband magnetosonic waves. However, the magnetosonic waves are exited with discrete narrowband spectra and electron transport response to such narrowband MS waves is still unclear.

In this study, we put forward a test particle simulation model with narrowband MS waves and investigate the relationship between bounce resonance coefficients and wave and background parameters. This paper is organized as follows. We will introduce the governing equations for particle motion, the wave model and the transport coefficients formulas in Section 2 and the simulation results of the parametric study will be presented in Section 3. In Section 4, there will be our conclusions and further discussion.

2 Test Particle Model

A mathematical model for relativistic electron motion in obliquely propagating whistler waves was developed by Tao and Bortnik (2010) by using gyrophase average and assuming a small wave amplitude compared with the background field. Chen et al. (2015) adopted it for the case of interaction between equatorially mirroring electrons and MS waves, where the gyroresonance and harmonic gyroresonance can be neglected. Extensions of multiple waves and random initial phases were applied in Maldonado et al. (2016); Maldonado and Chen (2018). Here we applied the gyro-phase averaged equations of motion in Chen and Bortnik (2020) for charged particles near an arbitrary resonance n in a set of waves with arbitary wave polarization in field-aligned coordinate system.

$$\begin{aligned}\frac{dp_z}{dt} &= -\frac{p_\perp^2}{2\gamma m B_0}\frac{dB_0}{dz} + g(\lambda, t) \\ &\times \sum_j \left[\frac{q e^{i\phi_{j,n}}}{2} \left(\widetilde{E}_{z,j} J_n + i v_\perp \widetilde{B}_{-,j} J_{n+1} e^{i\psi_j} - i v_\perp \widetilde{B}_{+,j} J_{n-1} e^{-i\psi_j} \right) + c.c. \right] \end{aligned} \tag{1}$$

$$\frac{dp_\perp}{dt} = +\frac{p_z p_\perp}{2\gamma m B_0}\frac{dB_0}{dz} + g(\lambda,t)$$
$$\times \sum_j \left[\frac{qe^{\phi_{j,n}}}{2}\left((\widetilde{E}_{-,j} - iv_z\widetilde{B}_{-,j}))J_{n+1}e^{i\psi_j} + (\widetilde{E}_{+,j} + iv_z\widetilde{B}_{+,j}J_{n-1}e^{-i\psi_j})\right) + c.c.\right] \quad (2)$$

$$\frac{d\phi_{j,n}}{dt} = n\Omega - \omega_j + k_{z,j}\cdot v_z + k_{\perp,j}\cdot v_d + g(\lambda,t)$$
$$\times n\sum_j \left[\frac{qe^{i\phi_{j,n}}}{2}\left(\frac{\widetilde{E}_{-,j} - iv_z\widetilde{B}_{-,j}}{-ip_\perp}J_{n+1}e^{i\psi_j} + \frac{\widetilde{E}_{-,j} + iv_z\widetilde{B}_{-,j}}{ip_\perp}J_{n-1}e^{-i\psi_j} - \frac{\widetilde{B}_{z,j}}{\gamma m}J_n\right) + c.c.\right]$$
$$(3)$$

$$\frac{dz}{dt} = v_z \quad (4)$$

The z is oriented with the background field, which is assumed to be dipolar with equatorial magnetic amplitude as B_0, and z is the arc distance of the field line from the magnetic equator. $B_0 = B_E\sqrt{1+3\sin^2\lambda}/(\cos^3\lambda\cdot L^3)$, where B_E is the Earth equator surface magnetic field magnitude, λ is the latitude and L is the L-shell value. x and y are two other perpendicular directions. m is the particle's mass and q is the charge, with the positive sign for ions and the negative for electrons. $p_\perp(v_\perp)$, $p_z(v_z)$ are the particle's perpendicular and parallel momentum(velocity) respectively and γ is the Lorentz factor. $\Omega = qB_0/\gamma m$ is the particle's gyrofrequency. The subscript j represents the jth wave component, with wave frequency ω_j, azimuthal angle ψ_j, perpendicular and parallel wave number $k_{\perp,j}$ and $k_{z,j}$. $\widetilde{B}$ and $\widetilde{E}$ are the wave magnetic and electric field complex amplitude and the wave components in a rotating coordinate system are $\widetilde{B}_{\pm,j} = (\widetilde{B}_{x,j}\pm i\widetilde{B}_{y,j})/2$, $\widetilde{E}_{\pm,j} = (\widetilde{E}_{x,j}\pm i\widetilde{E}_{y,j})/2$. The *c.c.* terms are the complex conjugate of the wave force terms. The terms $J_n(\beta_j)$ represent first kind Bessel functions with argument $\beta_j = k_{\perp,j}p_\perp/qB_0$. $\phi_{j,n}$ is the phase difference between jth wave and nth multiple of gyrophase. $g(\lambda,t) = g_\lambda(\lambda)g_t(t)$ is the scale factor of magnetic latitude λ and time t. The definitions of $g(\lambda)$ and $g(t)$ are shown in Equation 5 and 6. $g_\lambda(\lambda)$ represents the wave power latitudinal distribution with Gaussian width λ_w. The time factor $g_t(t)$ is used to describe the wave temporal amplitude variation, with t_1, t_2 as the wave's initial and final time point and $\Delta t_1, \Delta t_2$ as the corresponding transition time scales. The time scale $\tau = t_2 - t_1$ is much less than the electron drift period τ_d and usually set as several bounce periods.

$$g_\lambda(\lambda) = \exp(-\frac{\lambda^2}{\lambda_w^2}) \quad (5)$$

$$\begin{aligned} &= \exp(-\frac{(t-t_1)^2}{\Delta t_1^2}),\ t < t_1 \\ g_t(t) &= 1,\ t_1 \le t \le t_2 \\ &= \exp(-\frac{(t-t_2)^2}{\Delta t_2^2}),\ t > t_2 \end{aligned} \quad (6)$$

This equation set include relativistic motion via Lorentz factor γ, the adiabatic effect due to dipolar background magnetic field $B_0(z)$, finite Larmor radius effects represented by J_n terms, transit scattering effect due to $g_\lambda(\lambda)$, Landau resonance effect due to $k_{z,j} \cdot v_z - \omega_j$ and bounce resonance. To understand the underlying physics associated with bounce resonance, here we apply the simplified governing bounce motion equation for a single wave in Chen et al. (2015):

$$\frac{dp_z}{dt} = -\frac{\mu}{\gamma}\frac{\partial B_0(z)}{\partial z} + \sin(\omega t - k_z z + \phi_0)\left(-J_0(\beta) e E_z^w - \frac{2J_1(\beta)}{\beta}\frac{B_z^w k_z \mu}{\gamma}\right) g(\lambda) \qquad (7)$$

in which μ is the magnetic momentum, ϕ_0 is initial phase difference between wave and gyrophase. Chen et al. (2015) used a wave model with a single wave phase and assumed μ and γ are conserved to the first order of p_z, which are reasonable for nearly equatorially mirroring electrons.

We will use this test particle simulation model to investigate equatorially mirroring energetic electron transport coefficients. We constructed a set of equally spacing discrete magnetic field waves with frequency range δf and center frequency f_0. The total power of the wave set is denoted by the root-mean-square value B_{wrms}. The number of waves in the set is N_w, which we always choose a large value so that the wave power spectrum density is independent of N_w. In this simulation, we choose $N_w = 100$. To simulate the nearly perpendicular propagating MS wave fields, we choose a wave normal angle θ_0 near 90° and wave frequency between the proton gyrofrequency f_{cp} and the lower hybrid resonance frequency f_{LHR}. The value of λ_w is set small to represent the equatorial confinement of magnetosonic waves. By the cold plasma dispersion relation for MS waves, we can obtain the wave vector $\mathbf{k}$ and wave electric field based on the magnetic field we set up. Each wave in the wave set is arranged with 100 random initial phases at the equator between 0 and 360°. The electrons are initialized with 101 equally spacing bounce phases, which are related to the electrons' latitude position, so we can simulate the bounce resonance effect with different wave and particle phases. The L-shell L will be used to describe the background dipole field, and plasma density N_0 is used to describe the background plasma environment. The plasma density N_0 can be set as constant for simplicity, considering that the MS waves are confined within a few degrees of the magnetic equator. In sum, four parameters will be considered to describe the wave magnetic field model, including root-mean-square of wave magnetic amplitude B_{wrms}, center frequency f_0, frequency width δf, latitudinal distribution width λ_w and wave normal angle θ_0, and two parameters will be used to describe the background environment, L-shell L and plasma density N_0. We will investigate the dependence of electron responses on these six parameters.

The followings are the simulation parameter settings for the nominal case. The wave frequency range is from $0.9 f_{b0}$ to $1.1 f_{b0}$, in which f_{b0} is the bounce frequency of an electron with 300 keV and 60 deg pitch angle at the equator and $f_{b0} = 2.36$ Hz. Thus the center frequency $f_0 = 1.0 f_{b0}$ and the frequency width $\delta f = 0.2 f_{b0}$. The magnetic wave amplitude is $B_{wrms} = 50$ pT, the wave normal angle is $\theta_0 = 88$ deg, and the latitudinal width is $\lambda_w = 3$ deg. As to $g_t(t)$, $t_1 = 1$ s,$\Delta t_1 = 0.1$ s,$t_2 = 200$ s, $\Delta t_2 = 3$ s. The electron energy range in this simulation is from 1 keV to 10 MeV, which covers the energy magnitude range of electrons in the radiation belt. The background parameters L-shell value is $L = 4.8$ and plasma number density $N_0 = 300$ cm^{-3}. With all the above settings, we simulate the particle's distribution responses in $\alpha_{eq}(t)$ and $E(t)$ over a time period of $\tau = 4$ s. Such a choice of τ ensures the electrons of interest bounce multiple cycles and the bounce resonance effect can be evaluated afterward. Figure 1 gives the test particle simulation result of the nominal case. The resonant interaction depends on the particle bounce phases and wave phases and this is a stochastic process. Thus we repeat the calculation 10,100 times(101 wave phases and 100 bounce phases have been used) and obtain the time evolution of the probability distribution for α_{eq} and E. The probability distribution function $P(\alpha_{eq0}, E_0, t; \alpha_{eq}, E)$, through binning α_{eq} and E values at time t, describes the likelihood for electrons with initial energy and equatorial pitch angle (α_{eq0}, E_0) to have (α_{eq}, E) at time t. The 2D probability is defined as $P(\alpha_{eq0}, E_0, t; \alpha_{eq}, E)\Delta\alpha_{eq}\Delta E$, where $\Delta\alpha_{eq}$ and ΔE denote the bin size of initial α_{eq} and E respectively. The 1D prob-

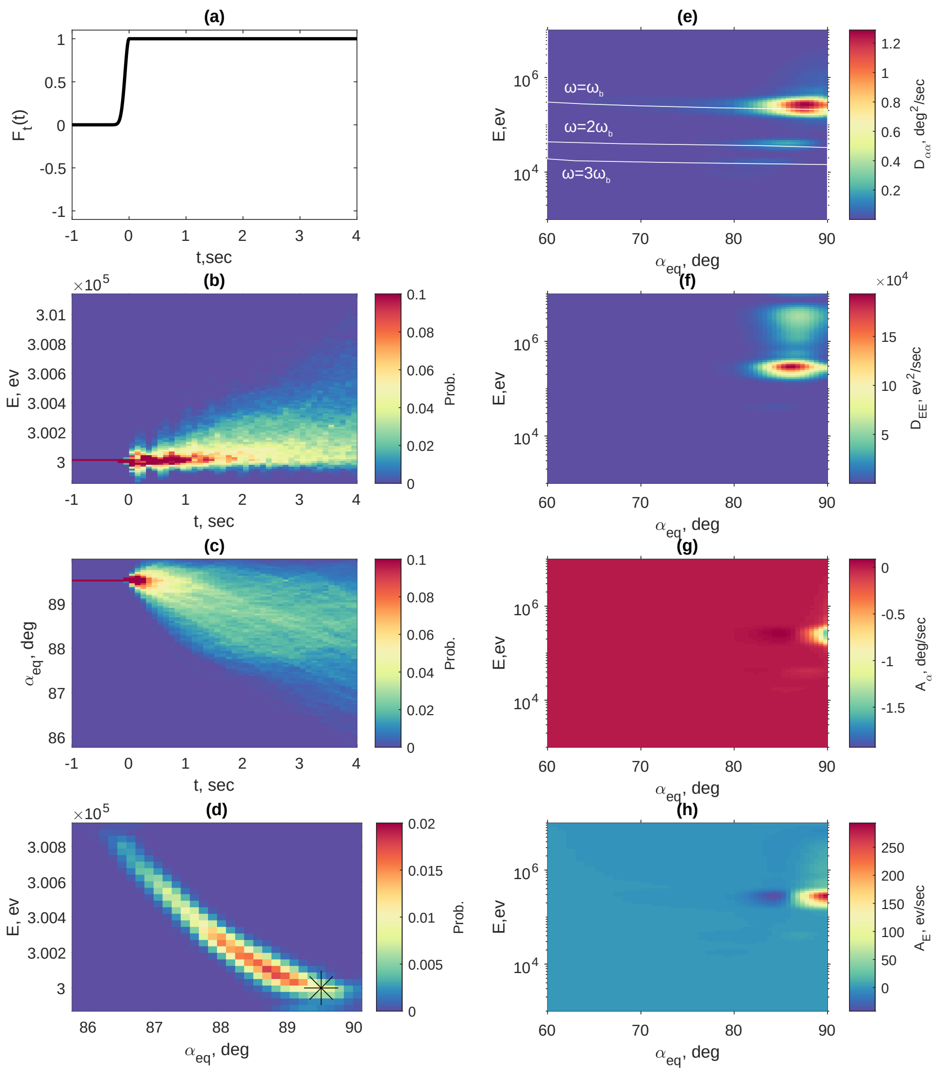

Figure 1. (a-d):Test particle simulation results with initial equatorial pitch angle $\alpha_{eq} = 89.5$ deg and initial energy $E_0 = 300$ keV. The parameter settings are:$\delta f = 0.2 f_{b0}, f_0 = 1.0 f_{b0}, \lambda_w = 3deg, \theta_0 = 88deg, B_{wrms} = 50pT, L = 4.8, N_0 = 300cm^{-3}$. The colorbars in (b-d) represent the electron distribution possibility. (a)Time profile of wave field. (b)Probability as a function of Energy E and time t: $Prob = P(\alpha_{eq0}, E_0, t; E)\Delta E$. (c)Probability as a function of equatorial pitch angle α_{eq} and time t: $Prob = P(\alpha_{eq0}, E_0, t; \alpha_{eq})\Delta\alpha_{eq}$. (d)Probability as a function of energy E and equatorial pitch angle α_{eq} at time $t = \tau = 4$ s.The asterisk represents the initial electrons probability distribution. (e-h):Four transport coefficients calculated with the same parameter settings as the model in (a-d) but with the energy range $E_0 \in (10^3, 10^7)eV$ and pitch angle range $\alpha_{eq} \in (60, 90)deg$. The colorbars in (e-h) represent the corresponding transport coefficient value. (e)The pitch angle diffusion coefficient $D_{\alpha\alpha}$ as a function of energy E and equatorial pitch angle α_{eq}. The three white solid lines denote the bounce resonance conditions for the first three harmonics, $\omega = \omega_b, \omega = 2\omega_b, \omega = 3\omega_b$. (f)The energy diffusion coefficient D_{EE} as a function of energy E and equatorial pitch angle α_{eq}. (g)The pitch angle advection coefficient A_α as a function of energy E and equatorial pitch angle α_{eq}. (h)The pitch angle advection coefficient A_E as a function of energy E and equatorial pitch angle α_{eq}.

ability function of α_{eq} or E is defined by the integral of the 2D probability function, and the explicit expressions are $P(\alpha_{eq0}, E_0, t; \alpha_{eq}) = \int P(\alpha_{eq0}, E_0, t; \alpha_{eq}, E)dE$, $P(\alpha_{eq0}, E_0, t; E) = \int P(\alpha_{eq0}, E_0, t; \alpha_{eq}, E)d\alpha_{eq}$. Figure 1(a-d) shows one example in that we initialize particles with a given $\alpha_{eq0} = 89.5$ deg and $E_0 = 300$ keV and then turn on the waves at $t = 0$, which is shown in Figure 1(a), and the time evolution of probability distribution of E and α_{eq} are shown in Figure 1(b) and (c), respectively. Figure 1 (d) shows an example of $P(\alpha_{eq0}, E_0, t; \alpha_{eq}, E)$ as a function of E and α_{eq} at time $t = \tau$, with the initial $\alpha_{eq0} = 89.5°$ and $E_0 = 300$ keV, which are represented by the asterisk.

As we can see, the particles are scattered from the initial energy 300 keV and initial equatorial pitch angle $\alpha_{eq} = 89.5$ deg. The transport process has two simultaneous effects, diffusion and advection. The former is the probability distribution broadening process in α_{eq} and E with time and the latter is the drifting of the peak probability of α_{eq} and E with time. These two transport coefficients are used to quantify the electron scattering effect. The diffusion coefficients of pitch angle and energy (Maldonado & Chen, 2018) are defined as:

$$D_{\alpha\alpha} = \frac{(\alpha_{eq} - [\alpha_{eq}])^2}{2t} \tag{8}$$

$$D_{EE} = \frac{(E - [E])^2}{2t} \tag{9}$$

The advection coefficients of pitch angle and energy are defined as:

$$A_{\alpha} = \frac{(\alpha_{eq} - [\alpha_{eq}])}{t} \tag{10}$$

$$A_{E} = \frac{(E - [E])}{t} \tag{11}$$

The operator [...] represents the ensemble average of α_{eq} or E over bounce phases and waves phases and its definition is

$$[Q] = \int\int d\alpha_{eq} dE \times Q \times P(\alpha_{eq0}, E_0, t; \alpha_{eq}, E) \tag{12}$$

Thus the transport coefficients can be described as a 2D function of (α_{eq0}, E_0) by calculating test particle simulation with different initial conditions. Figure 1 (e-f) present the four transport coefficients: the energy and pitch angle diffusion and advection coefficients at time $t = 4$s. One can clearly see that the diffusion coefficients $D_{\alpha\alpha}$ and D_{EE} reach their peaks around $\alpha_{eq0} = 85$ deg around 300 keV (Figure 1(e)(f)) while significant negative A_α and positive A_E appears near $\alpha_{eq0} = 90$ deg. One can expect that electrons with higher pitch angles have bigger transport coefficients since they have lower mirror latitude and will be accelerated with MS wave field more efficiently than those with lower pitch angles. Since we choose the wave center frequency $f_0 = f_{b0}$, no wonder the coefficients peaks locate around the energy around 300 keV, which satisfies the bounce resonant condition $\omega = \omega_b$.

One can clearly see multiple peaks in each coefficient in Figure 1(e-h) resulting from bounce resonance harmonics. In Figure 1(e), we plot the pitch angle diffusion coefficient together with bounce resonance harmonics conditions. We can see that the peaks in energy match with the harmonic bounce resonance condition $\omega = n\omega_b$, in which ω_b means the electron bounce angular frequency and n is a positive integer and represents the bounce harmonic order. We present the first three harmonics and find that different bounce harmonic resonances correspond to different peaks in the transport coefficients. Higher order harmonic resonances exist but the effect of fundamental resonance is much stronger. This is consistent with the conclusion in (Chen et al., 2015). Thus to achieve the most efficient bounce resonance transport effect to remove equatorially mirroring electrons away from oblique pitch angle, the low harmonic resonant condition should be satisfied.

We can compare the relative importance between diffusion and advection effect by calculating $\sqrt{D_{\alpha\alpha} \cdot t}$ and $|A_\alpha \cdot t|$. For example, to compare the two pitch angle transport effect of particles with 1 MeV and $\alpha_{eq0} = 90$ deg, $\sqrt{D_{\alpha\alpha} \cdot t} = \sqrt{0.02 \times 4}$ deg $\ll |A_\alpha \cdot t| = |-0.30 \times 4|$ deg, which means that the advection dominates over diffusion in this case. One can also compare the relative importance between pitch angle diffusion and energy diffusion effect by calculating $D_{\alpha\alpha}$ and D_{EE}/E^2. Take the peak point in $D_{\alpha\alpha}$ and D_{EE} as an example. $D_{\alpha\alpha} \approx 1.2$ and $D_{EE}/E^2 \approx 2 \cdot 10^5/(3 \cdot 10^5)^2 \approx 10^{-6}$, thus we can get that the pitch angle diffusion is more important than energy diffusion. A similar comparison can be done for A_α and A_E by calculating $|A_\alpha|$ and $|A_E/E|$ and find the similar conclusion that pitch angle advection is more obvious than energy advection. This can be understood by using μ conservation. Since $\mu = E \sin \alpha_{eq}^2 / B_{eq}$ is conserved, $|\Delta\alpha_{eq}/\tan\alpha_{eq}| = |\Delta E/2E|$ and α_{eq} is near 90 deg, the relative change of α_{eq} is more significant than the relative change of ΔE. These peaks mean that the electrons are scattered most efficiently with corresponding energies and pitch angles under the given MS wave and background parameters. Considering that pitch angle transport is more important in this process, in the following parametric study section, pitch angle transport coefficients are more valuable to be investigated. The analytic diffusion coefficients for broadband waves have been obtained (Chen & Bortnik, 2020) but the advection coefficients remain little explored. And for $\alpha_{eq0} < 80$ deg, diffusion dominates over advection, while the response of nearly equatorially mirroring electrons is nonlinear with significant advection. Thus, we will use the A_α to represent the transport coefficients and their peaks to identify the most effective transport conditions of electrons energy and pitch angle in the following parametric study.

3 Parametric Study

In this section, we investigate the dependencies of the transport effect, which is represented by advection coefficient A_α, on the background and wave parameters, namely, root-mean-square wave magnetic amplitude B_{wrms}, center frequency f_0, frequency width δf, latitudinal distribution width λ_w, wave normal angle θ_0, L-shell value and plasma density N_0. Each time we will vary one parameter while keeping the others the same as the nominal case in Figure 1.

3.1 Wave Frequency Width δf

In Figure 2, we present the advection coefficient A_α together with the harmonic bounce resonance conditions. Figure 2(a-c) present the comparison of transport coefficient A_α with different wave frequency widths. When the frequency width δf is small, the wave can be seen as a monochromatic wave and different harmonic resonances effects are separate in energy. With δf increasing, the affected energy gets broader but the magnitude decreases, which means the bounce resonance transport effect will happen over a broad energy range but the effect itself decays. To understand why this happens, we need to use the simplified Equation (7). When the wave frequency width broadens, the frequency width for each discrete wave increases and the wave power spectrum density will decrease, the wave amplitude E_z^w and B_z^w will decrease, and the amplitude of the second term on the right hand side of Equation (7) will decrease, which will weaken the resonance effect.

3.2 Wave Center Frequency f_0

Figure 2(d-f) show the comparison of transport coefficient A_α with different wave center frequency f_0. Higher order resonance harmonics will dominate and play a significant role in electron transportation. The fundamental in (d) and first two harmonics in (e) disappear because the electron's bounce frequency has an upper limit due to relativistic effect and the resonant condition cannot be satisfied any more. By comparing

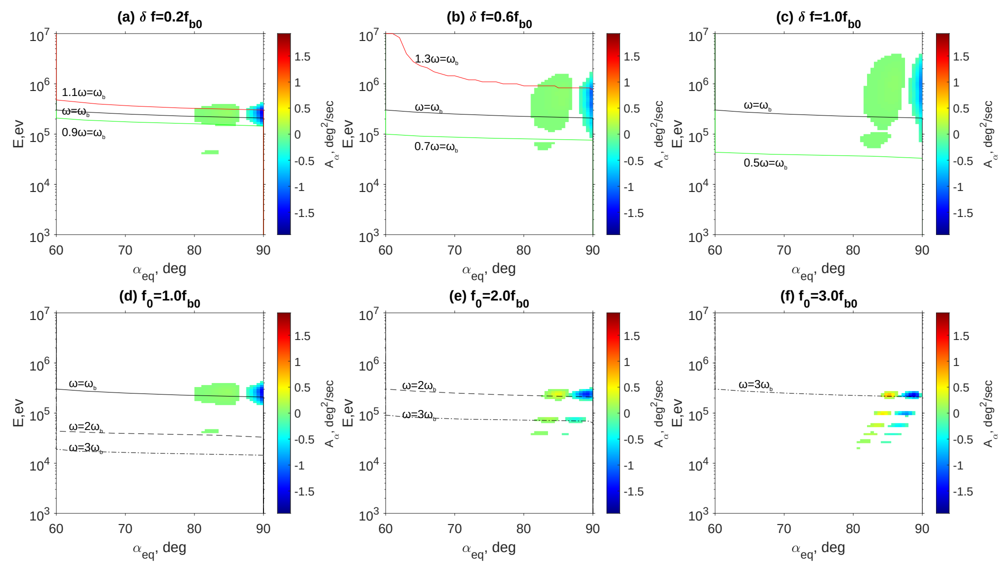

Figure 2. Transport coefficient A_α dependency on (a-c) frequency width and (d-f) center frequency. The red, black and green solid lines in (a-c) represent the wave frequency upper limit, center frequency and lower limit, respectively.The black solid, dashed, dot-dashed lines in (d-e) represent the bounce resonance conditions of $\omega = \omega_b, \omega = 2\omega_b, \omega = 3\omega_b$, respectively.

the peaks value in(d-f), one can see that the second(e) and the third(f) harmonic resonance transport effect in high wave frequency is comparable with the fundamental mode in low wave frequency. This is because when f_0 increases, the related $k_\perp$ decreases, $J_0(\beta)$ and $J_1(\beta)/\beta$ increase and will increase the amplitude of the second term on the right hand side of Equation (7).

3.3 Wave Latitudinal Distribution Width λ_w

Figure 3(a-c) shows the comparison of transport coefficient A_α with different latitudinal distribution width λ_w. One can see that A_α decreases with λ_w at first and then increases. Increasing λ_w enhances the wave power over a longer bouncing path and increases the transport but the transit time scattering (Bortnik & Thorne, 2010) may decrease as λ_w increases.

3.4 Wave Normal Angle θ_0

Figure 3(d-f) shows the comparison of transport coefficient A_α with different wave normal angle θ_0. One can easily find that with θ_0 increasing, A_α decreases. With increasing θ_0, β increases and k_z decreases and the amplitude of the second term on the right hand side of Equation (7) decreases, which will weaken the transport effect.

3.5 Root-Mean-Square Value of Wave Magnetic Field B_{wrms}

Figure 3(g-i) shows the comparison of transport coefficient A_α with different wave magnetic field amplitude B_{wrms}. Clearly, the transport coefficient A_α increases with B_{wrms} increasing. It is not surprising to get this result as E_z^w and B_z^w in the second term on

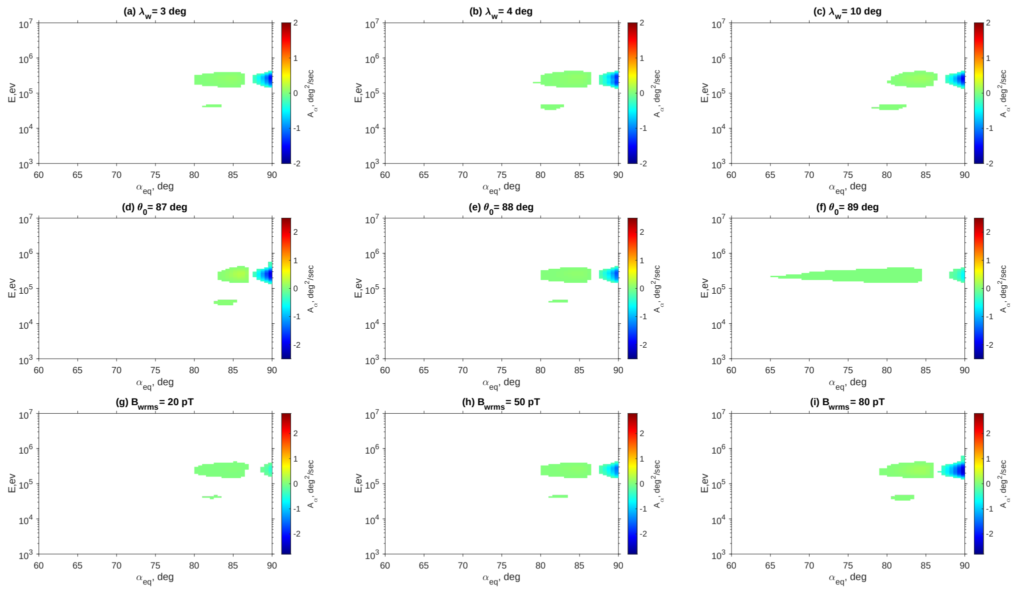

Figure 3. Transport coefficient A_α dependency on (a-c) wave latitudinal distribution width λ_w, (d-f) wave normal angle θ_0 and (g-i) root-mean-square of magnetic field amplitude B_{wrms}.

the right hand side of equation 7 will both increase. Furthermore, we can also find that the transport effect is linear with the wave amplitude since $dp_z/dt \propto E_z^W, B_z^w$, which has been verified but not shown here.

3.6 *L*-shell Value

Usually, L-shell value and plasma density N_0 are correlated since plasma density drops in order of magnitude at plasmapause and inside the plasmasphere (low L) N_0 is much bigger than that outside the plasmasphere (high L). However, the irregularities of the plasmasphere, like plumes, make it possible to have low L and low N_0, high L and high N_0. Therefore, we treat L and N_0 as independent variables. Figure 4 compares transport coefficient A_α with different L-shell value. We find that A_α increases when the L-shell value increases. Increasing L-shell value leads to higher μ since $\mu \propto L^3$, and will increase the amplitude of the second term on the right hand side of equation 7.

3.7 Plamsa Density N_0

We choose three typical values of N_0 to compare the transport coefficient A_α. $N_0 = 300, 100, 10cm^{-3}$ represent the plasma density inside the plasmasphere, near plasmapause and outside the plasmasphere, respectively. It is apparent that transport coefficient A_α increases with N_0 increasing. According to the properties of MS waves, $\omega/k_\perp \approx V_A(N_0), k_\perp/k_z = tan(\theta_0)$, where V_A is the Alfven velocity. Increasing N_0 results in smaller V_A and thus larger $k_\perp$ and k_z. Although larger $k_\perp$ will decrease J_0 and J_1/β, k_z's importance dominates and the amplitude of the second term on the right hand side of equation 7 increases.

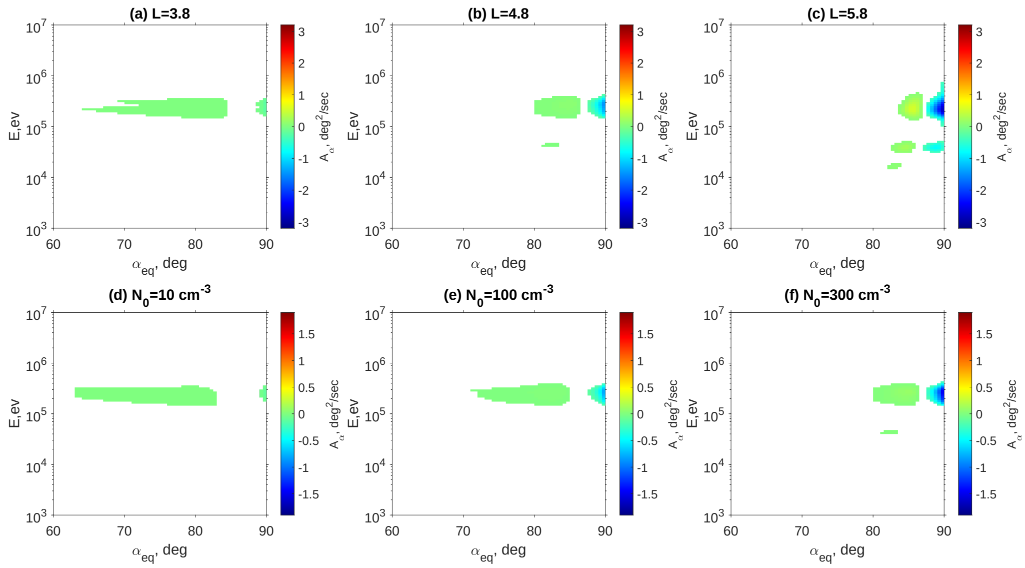

Figure 4. Transport coefficient A_α dependency on background parameters: (a-c) L-shell value and (d-f) plasma density N_0.

4 Conclusions and Discussion

In this study, we use test-particle simulation and investigate the equatorially mirroring electrons transport coefficients due to nonlinear bounce resonance with MS waves and its dependencies with wave field parameters (frequency width, center frequency, latitudinal width, wave normal angle and root-mean-square of wave amplitude) and background parameters (L-shell value and plasma density). Our principal conclusions are summarized as follows:

(1) Different bounce harmonic resonances correspond to different peaks in the transport coefficients. Higher order harmonic resonances exist but the effect of fundamental resonance is much stronger if present.

(2) With wave center frequency increasing, higher order harmonics start to dominate.

(3) The bounce resonance effect tends to increase with increasing latitudinal width, wave amplitude, L-shell value and plasma density, and decreasing wave normal angle and wave frequency width.

The diffusion or advection by bounce resonance with MS waves and parametric relationships in this study are expected to be incorporated into the radiation belt modeling. Previous modelings of electron diffusion pay main attention to gyroresonance with chorus or hiss waves, where the bounce motion is averaged and the bounce resonance effect is not considered (e.g. Xiao et al., 2009). The bounce resonance with MS waves should be taken into consideration (Chen et al., 2015; Tao et al., 2016) and our results of bounce diffusion can be implemented into the global simulation of electron diffusion. As to advection effect, the analytic expressions of advection coefficients remains unclear so far and the advection effect is usually not included in previous studies on electron transport. Zheng et al. (2021) proposed a numerical solver for Fokker-Planck equation of radiation belt, which contains the advection coefficients and provided a good framework to investigate the advection. It will be promising to use the adevetion coefficients calculated in this study as inputs of the model in Zheng et al. (2021) in the future.

The realistic MS waves usually have multiple equally spacing wave bands (Santolík et al., 2004; Min et al., 2018) while in this paper we consider only one wave frequency band in the wave model. Tao et al. (2013) investigated the amplitude modulation of a two-wave model for whistler mode waves and found the resonance overlap could result in different change of the electron pitch angle and energy from the ideal single-wave. An et al. (2014) established a two-wave model for electromagnetic ion cyclotron(EMIC) waves and adopted an oscillator dynamic system to understand the electron behavior. Compared with whistler mode waves and EMIC waves, MS waves have more obvious harmonic structures in frequency and the coherent interactions of electrons with MS waves needs to be investigated in the future.

Acknowledgments

References

An, X., Chen, L., Bortnik, J., & Thorne, R. M. (2014). An oscillator model representative of electron interactions with emic waves. *Journal of Geophysical Research: Space Physics*, *119*(3), 1951-1959. Retrieved from `https://agupubs.onlinelibrary.wiley.com/doi/abs/10.1002/2013JA019597` doi: https://doi.org/10.1002/2013JA019597

Blum, L., Artemyev, A., Agapitov, O., Mourenas, D., Boardsen, S., & Schiller, Q. (2019). Emic wave-driven bounce resonance scattering of energetic electrons in the inner magnetosphere. *Journal of Geophysical Research: Space Physics*, *124*(4), 2484-2496. Retrieved from `https://agupubs.onlinelibrary.wiley.com/doi/abs/10.1029/2018JA026427` doi: https://doi.org/10.1029/2018JA026427

Bortnik, J., & Thorne, R. M. (2010). Transit time scattering of energetic electrons due to equatorially confined magnetosonic waves. *Journal of Geophysical Research: Space Physics*, *115*(A7). Retrieved from `https://agupubs.onlinelibrary.wiley.com/doi/abs/10.1029/2010JA015283` doi: https://doi.org/10.1029/2010JA015283

Cao, X., Ni, B., Summers, D., Bortnik, J., Tao, X., Shprits, Y. Y., … Wang, Q. (2017). Bounce resonance scattering of radiation belt electrons by h+ band emic waves. *Journal of Geophysical Research: Space Physics*, *122*(2), 1702-1713. Retrieved from `https://agupubs.onlinelibrary.wiley.com/doi/abs/10.1002/2016JA023607` doi: https://doi.org/10.1002/2016JA023607

Chen, L., & Bortnik, J. (2020). Chapter 4 - wave-particle interactions with coherent magnetosonic waves. In A. N. Jaynes & M. E. Usanova (Eds.), *The dynamic loss of earth's radiation belts* (p. 99-120). Elsevier. Retrieved from `https://www.sciencedirect.com/science/article/pii/B9780128133712000044` doi: https://doi.org/10.1016/B978-0-12-813371-2.00004-4

Chen, L., Maldonado, A., Bortnik, J., Thorne, R. M., Li, J., Dai, L., & Zhan, X. (2015). Nonlinear bounce resonances between magnetosonic waves and equatorially mirroring electrons. *Journal of Geophysical Research: Space Physics*, *120*(8), 6514-6527. Retrieved from `https://agupubs.onlinelibrary.wiley.com/doi/abs/10.1002/2015JA021174` doi: https://doi.org/10.1002/2015JA021174

Chen, L., & Thorne, R. M. (2012). Perpendicular propagation of magnetosonic waves. *Geophysical Research Letters*, *39*(14). Retrieved from `https://agupubs.onlinelibrary.wiley.com/doi/abs/10.1029/2012GL052485` doi: https://doi.org/10.1029/2012GL052485

Chen, L., Thorne, R. M., Jordanova, V. K., Thomsen, M. F., & Horne, R. B. (2011). Magnetosonic wave instability analysis for proton ring distributions observed by the lanl magnetospheric plasma analyzer. *Journal of Geophysical Research: Space Physics*, *116*(A3). Retrieved from https://agupubs.onlinelibrary.wiley.com/doi/abs/10.1029/2010JA016068 doi: https://doi.org/10.1029/2010JA016068

Gary, S. P., Liu, K., Winske, D., & Denton, R. E. (2010). Ion bernstein instability in the terrestrial magnetosphere: Linear dispersion theory. *Journal of Geophysical Research: Space Physics*, *115*(A12). Retrieved from https://agupubs.onlinelibrary.wiley.com/doi/abs/10.1029/2010JA015965 doi: https://doi.org/10.1029/2010JA015965

Gurnett, D. A. (1976). Plasma wave interactions with energetic ions near the magnetic equator. *Journal of Geophysical Research (1896-1977)*, *81*(16), 2765-2770. Retrieved from https://agupubs.onlinelibrary.wiley.com/doi/abs/10.1029/JA081i016p02765 doi: https://doi.org/10.1029/JA081i016p02765

Hanzelka, M., Němec, F., Santolík, O., & Parrot, M. (2022). Statistical analysis of wave propagation properties of equatorial noise observed at low altitudes. *Journal of Geophysical Research: Space Physics*, *127*(7), e2022JA030416. Retrieved from https://agupubs.onlinelibrary.wiley.com/doi/abs/10.1029/2022JA030416 (e2022JA030416 2022JA030416) doi: https://doi.org/10.1029/2022JA030416

Li, X., & Tao, X. (2018). Validation and analysis of bounce resonance diffusion coefficients. *Journal of Geophysical Research: Space Physics*, *123*(1), 104-113. Retrieved from https://agupubs.onlinelibrary.wiley.com/doi/abs/10.1002/2017JA024506 doi: https://doi.org/10.1002/2017JA024506

Li, X., Tao, X., Lu, Q., & Dai, L. (2015). Bounce resonance diffusion coefficients for spatially confined waves. *Geophysical Research Letters*, *42*(22), 9591-9599. Retrieved from https://agupubs.onlinelibrary.wiley.com/doi/abs/10.1002/2015GL066324 doi: https://doi.org/10.1002/2015GL066324

Liu, K., Gary, S. P., & Winske, D. (2011). Excitation of magnetosonic waves in the terrestrial magnetosphere: Particle-in-cell simulations. *Journal of Geophysical Research: Space Physics*, *116*(A7). Retrieved from https://agupubs.onlinelibrary.wiley.com/doi/abs/10.1029/2010JA016372 doi: https://doi.org/10.1029/2010JA016372

Liu, Z.-Y., Zong, Q.-G., Zhou, X.-Z., Zhu, Y.-F., & Gu, S.-J. (2020). Pitch angle structures of ring current ions induced by evolving poloidal ultra-low frequency waves. *Geophysical Research Letters*, *47*(4), e2020GL087203. Retrieved from https://agupubs.onlinelibrary.wiley.com/doi/abs/10.1029/2020GL087203 (e2020GL087203 10.1029/2020GL087203) doi: https://doi.org/10.1029/2020GL087203

Ma, Q., Li, W., Thorne, R. M., & Angelopoulos, V. (2013). Global distribution of equatorial magnetosonic waves observed by themis. *Geophysical Research Letters*, *40*(10), 1895-1901. Retrieved from https://agupubs.onlinelibrary.wiley.com/doi/abs/10.1002/grl.50434 doi: https://doi.org/10.1002/grl.50434

Maldonado, A. A., & Chen, L. (2018). On the diffusion rates of electron bounce resonant scattering by magnetosonic waves. *Geophysical Research Letters*, *45*(8), 3328-3337. Retrieved from https://agupubs.onlinelibrary.wiley.com/doi/abs/10.1002/2017GL076560 doi: https://doi.org/10.1002/2017GL076560

Maldonado, A. A., Chen, L., Claudepierre, S. G., Bortnik, J., Thorne, R. M., & Spence, H. (2016). Electron butterfly distribution modulation by magnetosonic waves. *Geophysical Research Letters*, *43*(7), 3051-3059. Retrieved from https://agupubs.onlinelibrary.wiley.com/doi/abs/10.1002/2016GL068161 doi: https://doi.org/10.1002/2016GL068161

Min, K., Liu, K., Wang, X., Chen, L., & Denton, R. E. (2018). Fast magnetosonic waves observed by van allen probes: Testing local wave excitation mechanism. *Journal of Geophysical Research: Space Physics*, *123*(1), 497-512. Retrieved from https://agupubs.onlinelibrary.wiley.com/doi/abs/10.1002/2017JA024867 doi: https://doi.org/10.1002/2017JA024867

Roberts, C. S., & Schulz, M. (1968). Bounce resonant scattering of particles trapped in the earth's magnetic field. *Journal of Geophysical Research (1896-1977)*, *73*(23), 7361-7376. Retrieved from https://agupubs.onlinelibrary.wiley.com/doi/abs/10.1029/JA073i023p07361 doi: https://doi.org/10.1029/JA073i023p07361

Russell, C. T., Holzer, R. E., & Smith, E. J. (1969). Ogo 3 observations of elf noise in the magnetosphere: 1. spatial extent and frequency of occurrence. *Journal of Geophysical Research (1896-1977)*, *74*(3), 755-777. Retrieved from https://agupubs.onlinelibrary.wiley.com/doi/abs/10.1029/JA074i003p00755 doi: https://doi.org/10.1029/JA074i003p00755

Santolík, O., Němec, F., Gereová, K., Macúšová, E., de Conchy, Y., & Cornilleau-Wehrlin, N. (2004). Systematic analysis of equatorial noise below the lower hybrid frequency. *Annales Geophysicae*, *22*(7), 2587–2595. Retrieved from https://angeo.copernicus.org/articles/22/2587/2004/ doi: 10.5194/angeo-22-2587-2004

Shprits, Y. Y. (2009). Potential waves for pitch-angle scattering of near-equatorially mirroring energetic electrons due to the violation of the second adiabatic invariant. *Geophysical Research Letters*, *36*(12). Retrieved from https://agupubs.onlinelibrary.wiley.com/doi/abs/10.1029/2009GL038322 doi: https://doi.org/10.1029/2009GL038322

Tao, X., & Bortnik, J. (2010). Nonlinear interactions between relativistic radiation belt electrons and oblique whistler mode waves. *Nonlinear Processes in Geophysics*, *17*(5), 599–604. Retrieved from https://npg.copernicus.org/articles/17/599/2010/ doi: 10.5194/npg-17-599-2010

Tao, X., Bortnik, J., Albert, J., Thorne, R., & Li, W. (2013). The importance of amplitude modulation in nonlinear interactions between electrons and large amplitude whistler waves. *Journal of Atmospheric and Solar-Terrestrial Physics*, *99*, 67-72. Retrieved from https://www.sciencedirect.com/science/article/pii/S1364682612001411 (Dynamics of the Complex Geospace System) doi: https://doi.org/10.1016/j.jastp.2012.05.012

Tao, X., Zhang, L., Wang, C., Li, X., Albert, J. M., & Chan, A. A. (2016). An efficient and positivity-preserving layer method for modeling radiation belt diffusion processes. *Journal of Geophysical Research: Space Physics*, *121*(1), 305-320. Retrieved from https://agupubs.onlinelibrary.wiley.com/doi/abs/10.1002/2015JA022064 doi: https://doi.org/10.1002/2015JA022064

Tsurutani, B. T., Falkowski, B. J., Pickett, J. S., Verkhoglyadova, O. P., Santolik, O., & Lakhina, G. S. (2014). Extremely intense elf magnetosonic waves: A survey of polar observations. *Journal of Geophysical Research: Space Physics*, *119*(2), 964-977. Retrieved from https://agupubs.onlinelibrary.wiley.com/doi/abs/10.1002/2013JA019284 doi: https://doi.org/10.1002/2013JA019284

Xiao, F., Su, Z., Zheng, H., & Wang, S. (2009). Modeling of outer radiation belt electrons by multidimensional diffusion process. *Journal of Geophysical Research: Space Physics*, *114*(A3). Retrieved from https://agupubs.onlinelibrary.wiley.com/doi/abs/10.1029/2008JA013580 doi: https://doi.org/10.1029/2008JA013580

Zheng, L., Chen, L., Chan, A. A., Wang, P., Xia, Z., & Liu, X. (2021). Uber v1.0: a universal kinetic equation solver for radiation belts. *Geoscientific Model Development*, *14*(9), 5825–5842. Retrieved from https://gmd.copernicus.org/articles/14/5825/2021/ doi: 10.5194/gmd-14-5825-2021

Zhu, Y.-F., Gu, S.-J., Zhou, X.-Z., Zong, Q.-G., Ren, J., Sun, X.-R., . . . Rankin, R. (2020). Drift-bounce resonance between charged particles and ultralow frequency waves: Theory and observations. *Journal of Geophysical Research: Space Physics*, *125*(1), e2019JA027067. Retrieved from `https://agupubs.onlinelibrary.wiley.com/doi/abs/10.1029/2019JA027067` (e2019JA027067 10.1029/2019JA027067) doi: https://doi.org/10.1029/2019JA027067

Bounce Resonance between Energetic Electrons and Magnetosonic Waves: A Parametric Study

Shujie Gu[1] **and Lunjin Chen**[1]

[1]Department of Physics, W.B. Hanson Center for Space Sciences, University of Texas at Dallas, Richardson, TX, USA

Key Points:

- Higher order harmonic resonances are important with high wave center frequency.
- The bounce resonance effect tends to increase with increasing wave latitudinal width, wave amplitude, L-shell value and background plasma density.
- Increasing wave normal angle and wave frequency width can decrease the bounce resonance effect.

Corresponding author: Shujie Gu, `shujie.gu@utdallas.edu`

Abstract

Magnetosonic waves are electromagnetic emissions from a few to 100 Hz primarily confined near the magnetic equator both inside and outside the plasmasphere. Previous studies proved that MS waves can transport equatorially mirroring electrons from an equatorial pitch angle of 90° down to lower values by bounce resonance. But the dependence of bounce resonance effect on wave or background plasma parameters is still unclear. Here we applied a test particle simulation to investigate electron transport coefficients, including diffusion and advection coefficients in energy and pitch angle, due to bounce resonance with MS waves. We investigate five wave field parameters, including wave frequency width, wave center frequency, latitudinal distribution width, wave normal angle and root-mean-square of wave magnetic amplitude, and two background parameters, L-shell value and plasma density. We find different transport coefficients peaks resulted by different bounce resonance harmonics. Higher order harmonic resonances exist, but the effect of fundamental resonance is much stronger. As the wave center frequency increases, higher order harmonics start to dominate. With wave frequency width increasing, the energy range of effective bounce resonance broadens, but the effect itself weakens. The bounce resonance effect will increase when we decrease the wave normal angle, or increase the wave amplitude, latitudinal distribution width, L-shell value, and plasma density. The parametric study will advance our understanding of the favorable conditions of bounce resonance.

Plain Language Summary

There are various plasma waves and wave-particle interactions in the magnetosphere and they are crucial for magnetosphere dynamics. Bounce resonance between electrons and magnetosonic waves is one of them and plays an essential role in removing equatorially mirroring electrons. Magnetosonic waves are electromagnetic emissions from several Hz to 100 Hz confined near the magnetic equator. The energetic electrons can be scattered by magnetosonic waves by bounce resonance. In this study, we run a test particle simulation and investigate the bounce resonance effective regime. The wave and background parameters are studied, including root-mean-square of wave magnetic amplitude, wave frequency width, center frequency, latitudinal width, wave normal angle, plasma density and$L$-shell value. The parametric study will improve our modeling of radiation belt dynamics.

1 Introduction

Magnetosponic(MS) waves, also called as equatorial noise (Russell et al., 1969) or equatorial MS waves (Ma et al., 2013), are ion Berstein mode waves driven by a proton velocity ring distribution with a positive slope in $\partial f_p(v)/\partial v_{perp}$ (Gary et al., 2010; K. Liu et al., 2011). They are magnetically compressional mode electromagnetic waves excited at very oblique wave normal angles and propagate nearly perpendicular to the background magnetic field (Chen et al., 2011; Chen & Thorne, 2012). Observationally, MS waves generally occur latitudinally near Earth's magnetic equator with a frequency range from the proton gyrofrequency f_{cp}(several Hz) to the lower hybrid frequency f_{LHR}(about 100 Hz) (Gurnett, 1976) and consist of discrete equally spacing spectral lines (Santolík et al., 2004; Min et al., 2018), which are multiples of f_{cp}. They are located both inside and outside the plasmasphere, and recent studies observed their occurrence in very low altitudes at the ionosphere with very strong geomagnetic activities(Hanzelka et al., 2022). The strong MS waves can be measured with the amplitudes of the dominant wave magnetic component around 50 pT for average cases (Ma et al., 2013) and 1 nT for extremely strong cases (Tsurutani et al., 2014).

Bounce resonance between electromagnetic waves and energetic particles have been well studied since Roberts and Schulz (1968) first formulated the theory. Bounce motion plays an important role in accelerating and scattering particles through wave-particle interactions with different waves in the magnetosphere, such as bounce resonance between EMIC waves and electrons with hundreds of keV (e.g. Blum et al., 2019; Cao et al., 2017) and drift-bounce resonance between Pc4-5 ULF waves and ions with tens of keV (e.g. Zhu et al., 2020; Z.-Y. Liu et al., 2020). Previous studies paid much more attention to gyroresonance and drift resonance interaction than bounce resonance. Equatorially mirroring energetic electrons, however, are generally immune to the gyroresonance interaction since it requires a finite parallel velocity along the field line to satisfy the gyroresonance condition when the electrons energies are not large enough to provide a sufficient relativistic Lorentz factor to reduce the gyrofrequency. But the observations have shown that equatorially mirroring electron flux in the radiation belt cannot build up continuously (Shprits, 2009).

To solve this problem, Chen et al. (2015) proposed a loss mechanism of equatorially mirroring electron by nonlinear bounce resonance between MS waves and equatorially mirroring energetic electrons, to account for the transportation of pitch angle from 90° to lower values, which enables the scattering of those electrons out of equatorial plane. The capability of removing equatorially mirroring electrons from 90° due to bounce resonance results in a butterfly distribution, a minimum at 90° in pitch angle distribution, observationally reported by Maldonado et al. (2016). Thus the bounce resonance transport process plays a vital role in electron scattering in radiation belt and the electron flux depletion during geomagnetic storms. The bounce resonance diffusion coefficients have been investigated through quasilinear diffusion theory and their formulas have been developed in a more realistic MS wave model, with the finite Larmor radius effect and Gaussian latitudinal distribution of wave intensity (Roberts & Schulz, 1968; Li et al., 2015; Tao et al., 2016; Li & Tao, 2018; Maldonado & Chen, 2018; Chen & Bortnik, 2020). The derived formulas are targeted for broadband magnetosonic waves. However, the magnetosonic waves are exited with discrete narrowband spectra and electron transport response to such narrowband MS waves is still unclear.

In this study, we put forward a test particle simulation model with narrowband MS waves and investigate the relationship between bounce resonance coefficients and wave and background parameters. This paper is organized as follows. We will introduce the governing equations for particle motion, the wave model and the transport coefficients formulas in Section 2 and the simulation results of the parametric study will be presented in Section 3. In Section 4, there will be our conclusions and further discussion.

2 Test Particle Model

A mathematical model for relativistic electron motion in obliquely propagating whistler waves was developed by Tao and Bortnik (2010) by using gyrophase average and assuming a small wave amplitude compared with the background field. Chen et al. (2015) adopted it for the case of interaction between equatorially mirroring electrons and MS waves, where the gyroresonance and harmonic gyroresonance can be neglected. Extensions of multiple waves and random initial phases were applied in Maldonado et al. (2016); Maldonado and Chen (2018). Here we applied the gyro-phase averaged equations of motion in Chen and Bortnik (2020) for charged particles near an arbitrary resonance n in a set of waves with arbitary wave polarization in field-aligned coordinate system.

$$\frac{dp_z}{dt} = -\frac{p_\perp^2}{2\gamma m B_0}\frac{dB_0}{dz} + g(\lambda, t)$$
$$\times \sum_j \left[\frac{q e^{i\phi_{j,n}}}{2} \left(\widetilde{E}_{z,j} J_n + i v_\perp \widetilde{B}_{-,j} J_{n+1} e^{i\psi_j} - i v_\perp \widetilde{B}_{+,j} J_{n-1} e^{-i\psi_j} \right) + c.c. \right] \tag{1}$$

$$
\begin{aligned}
&\frac{dp_\perp}{dt} = +\frac{p_z p_\perp}{2\gamma m B_0}\frac{dB_0}{dz} + g(\lambda,t) \\
&\times \sum_j \left[\frac{qe^{\phi_{j,n}}}{2}\left((\widetilde{E}_{-,j} - iv_z\widetilde{B}_{-,j}))J_{n+1}e^{i\psi_j} + (\widetilde{E}_{+,j} + iv_z\widetilde{B}_{+,j}J_{n-1}e^{-i\psi_j})\right) + c.c.\right]
\end{aligned} \tag{2}
$$

$$
\begin{aligned}
&\frac{d\phi_{j,n}}{dt} = n\Omega - \omega_j + k_{z,j}\cdot v_z + k_{\perp,j}\cdot v_d + g(\lambda,t) \\
&\times n\sum_j \left[\frac{qe^{i\phi_{j,n}}}{2}\left(\frac{\widetilde{E}_{-,j} - iv_z\widetilde{B}_{-,j}}{-ip_\perp}J_{n+1}e^{i\psi_j} + \frac{\widetilde{E}_{-,j} + iv_z\widetilde{B}_{-,j}}{ip_\perp}J_{n-1}e^{-i\psi_j} - \frac{\widetilde{B}_{z,j}}{\gamma m}J_n\right) + c.c.\right]
\end{aligned} \tag{3}
$$

$$
\frac{dz}{dt} = v_z \tag{4}
$$

The z is oriented with the background field, which is assumed to be dipolar with equatorial magnetic amplitude as B_0, and z is the arc distance of the field line from the magnetic equator. $B_0 = B_E\sqrt{1+3\sin^2\lambda}/(\cos^3\lambda\cdot L^3)$, where B_E is the Earth equator surface magnetic field magnitude, λ is the latitude and L is the L-shell value. x and y are two other perpendicular directions. m is the particle's mass and q is the charge, with the positive sign for ions and the negative for electrons. $p_\perp(v_\perp)$, $p_z(v_z)$ are the particle's perpendicular and parallel momentum(velocity) respectively and γ is the Lorentz factor. $\Omega = qB_0/\gamma m$ is the particle's gyrofrequency. The subscript j represents the jth wave component, with wave frequency ω_j, azimuthal angle ψ_j, perpendicular and parallel wave number $k_{\perp,j}$ and $k_{z,j}$. $\widetilde{B}$ and $\widetilde{E}$ are the wave magnetic and electric field complex amplitude and the wave components in a rotating coordinate system are $\widetilde{B}_{\pm,j} = (\widetilde{B}_{x,j}\pm i\widetilde{B}_{y,j})/2$, $\widetilde{E}_{\pm,j} = (\widetilde{E}_{x,j}\pm i\widetilde{E}_{y,j})/2$. The *c.c.* terms are the complex conjugate of the wave force terms. The terms $J_n(\beta_j)$ represent first kind Bessel functions with argument $\beta_j = k_{\perp,j}p_\perp/qB_0$. $\phi_{j,n}$ is the phase difference between jth wave and nth multiple of gyrophase. $g(\lambda,t) = g_\lambda(\lambda)g_t(t)$ is the scale factor of magnetic latitude λ and time t. The definitions of $g(\lambda)$ and $g(t)$ are shown in Equation 5 and 6. $g_\lambda(\lambda)$ represents the wave power latitudinal distribution with Gaussian width λ_w. The time factor $g_t(t)$ is used to describe the wave temporal amplitude variation, with t_1, t_2 as the wave's initial and final time point and $\Delta t_1, \Delta t_2$ as the corresponding transition time scales. The time scale $\tau = t_2 - t_1$ is much less than the electron drift period τ_d and usually set as several bounce periods.

$$
g_\lambda(\lambda) = \exp(-\frac{\lambda^2}{\lambda_w^2}) \tag{5}
$$

$$
\begin{aligned}
&= \exp(-\frac{(t-t_1)^2}{\Delta t_1^2}),\ t<t_1 \\
g_t(t) &= 1,\ t_1 \le t \le t_2 \\
&= \exp(-\frac{(t-t_2)^2}{\Delta t_2^2}),\ t>t_2
\end{aligned} \tag{6}
$$

This equation set include relativistic motion via Lorentz factor γ, the adiabatic effect due to dipolar background magnetic field $B_0(z)$, finite Larmor radius effects represented by J_n terms, transit scattering effect due to $g_\lambda(\lambda)$, Landau resonance effect due to $k_{z,j} \cdot v_z - \omega_j$ and bounce resonance. To understand the underlying physics associated with bounce resonance, here we apply the simplified governing bounce motion equation for a single wave in Chen et al. (2015):

$$\frac{dp_z}{dt} = -\frac{\mu}{\gamma}\frac{\partial B_0(z)}{\partial z} + \sin(\omega t - k_z z + \phi_0)\left(-J_0(\beta)eE_z^w - \frac{2J_1(\beta)}{\beta}\frac{B_z^w k_z \mu}{\gamma}\right)g(\lambda) \qquad (7)$$

in which μ is the magnetic momentum, ϕ_0 is initial phase difference between wave and gyrophase. Chen et al. (2015) used a wave model with a single wave phase and assumed μ and γ are conserved to the first order of p_z, which are reasonable for nearly equatorially mirroring electrons.

We will use this test particle simulation model to investigate equatorially mirroring energetic electron transport coefficients. We constructed a set of equally spacing discrete magnetic field waves with frequency range δf and center frequency f_0. The total power of the wave set is denoted by the root-mean-square value B_{wrms}. The number of waves in the set is N_w, which we always choose a large value so that the wave power spectrum density is independent of N_w. In this simulation, we choose $N_w = 100$. To simulate the nearly perpendicular propagating MS wave fields, we choose a wave normal angle θ_0 near 90° and wave frequency between the proton gyrofrequency f_{cp} and the lower hybrid resonance frequency f_{LHR}. The value of λ_w is set small to represent the equatorial confinement of magnetosonic waves. By the cold plasma dispersion relation for MS waves, we can obtain the wave vector $\mathbf{k}$ and wave electric field based on the magnetic field we set up. Each wave in the wave set is arranged with 100 random initial phases at the equator between 0 and 360°. The electrons are initialized with 101 equally spacing bounce phases, which are related to the electrons' latitude position, so we can simulate the bounce resonance effect with different wave and particle phases. The L-shell L will be used to describe the background dipole field, and plasma density N_0 is used to describe the background plasma environment. The plasma density N_0 can be set as constant for simplicity, considering that the MS waves are confined within a few degrees of the magnetic equator. In sum, four parameters will be considered to describe the wave magnetic field model, including root-mean-square of wave magnetic amplitude B_{wrms}, center frequency f_0, frequency width δf, latitudinal distribution width λ_w and wave normal angle θ_0, and two parameters will be used to describe the background environment, L-shell L and plasma density N_0. We will investigate the dependence of electron responses on these six parameters.

The followings are the simulation parameter settings for the nominal case. The wave frequency range is from $0.9f_{b0}$ to $1.1f_{b0}$, in which f_{b0} is the bounce frequency of an electron with 300 keV and 60 deg pitch angle at the equator and $f_{b0} = 2.36$ Hz. Thus the center frequency $f_0 = 1.0f_{b0}$ and the frequency width $\delta f = 0.2f_{b0}$. The magnetic wave amplitude is $B_{wrms} = 50$ pT, the wave normal angle is $\theta_0 = 88$ deg, and the latitudinal width is $\lambda_w = 3$ deg. As to $g_t(t)$, $t_1 = 1$ s,$\Delta t_1 = 0.1$ s,$t_2 = 200$ s, $\Delta t_2 = 3$ s. The electron energy range in this simulation is from 1 keV to 10 MeV, which covers the energy magnitude range of electrons in the radiation belt. The background parameters L-shell value is $L = 4.8$ and plasma number density $N_0 = 300$ cm^{-3}. With all the above settings, we simulate the particle's distribution responses in $\alpha_{eq}(t)$ and $E(t)$ over a time period of $\tau = 4$ s. Such a choice of τ ensures the electrons of interest bounce multiple cycles and the bounce resonance effect can be evaluated afterward. Figure 1 gives the test particle simulation result of the nominal case. The resonant interaction depends on the particle bounce phases and wave phases and this is a stochastic process. Thus we repeat the calculation 10,100 times(101 wave phases and 100 bounce phases have been used) and obtain the time evolution of the probability distribution for α_{eq} and E. The probability distribution function $P(\alpha_{eq0}, E_0, t; \alpha_{eq}, E)$, through binning α_{eq} and E values at time t, describes the likelihood for electrons with initial energy and equatorial pitch angle (α_{eq0}, E_0) to have (α_{eq}, E) at time t. The 2D probability is defined as $P(\alpha_{eq0}, E_0, t; \alpha_{eq}, E)\Delta\alpha_{eq}\Delta E$, where $\Delta\alpha_{eq}$ and ΔE denote the bin size of initial α_{eq} and E respectively. The 1D prob-

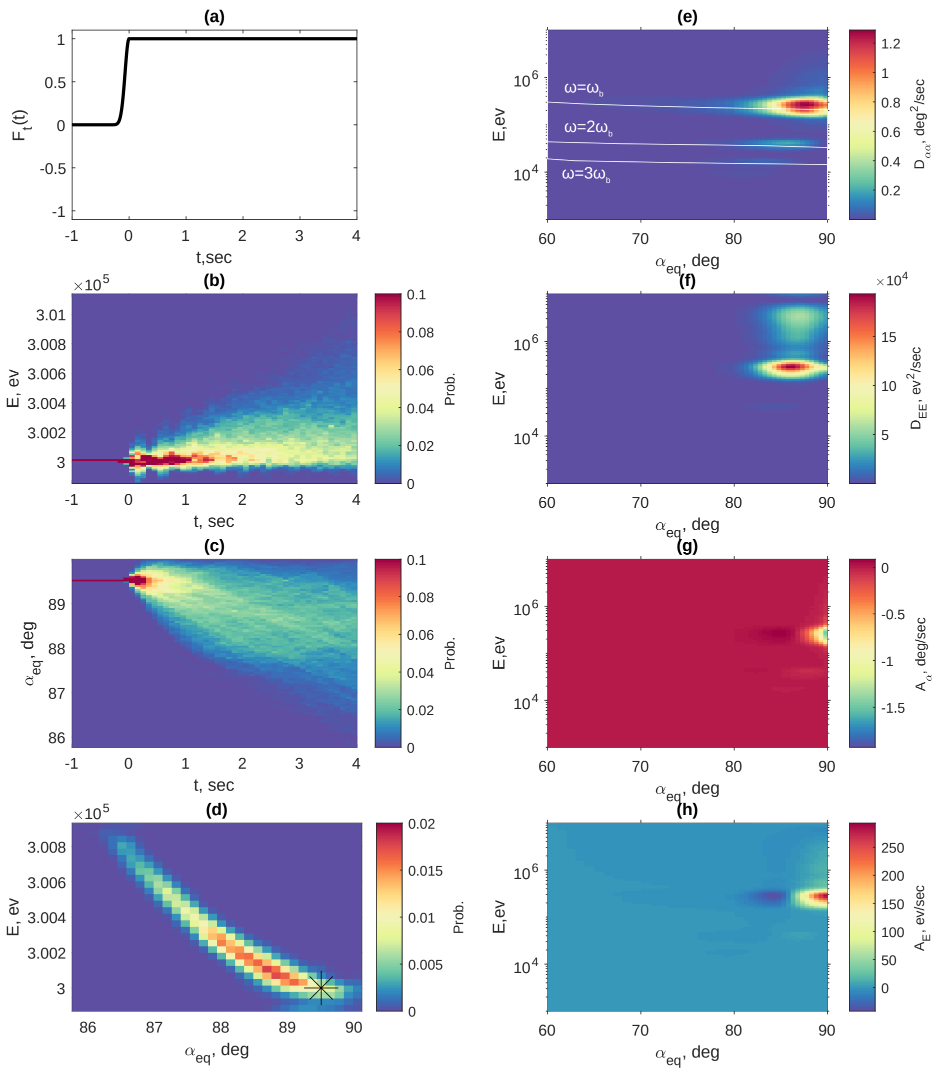

Figure 1. (a-d):Test particle simulation results with initial equatorial pitch angle $\alpha_{eq} = 89.5$ deg and initial energy $E_0 = 300$ keV. The parameter settings are:$\delta f = 0.2 f_{b0}, f_0 = 1.0 f_{b0}, \lambda_w = 3deg, \theta_0 = 88deg, B_{wrms} = 50pT, L = 4.8, N_0 = 300cm^{-3}$. The colorbars in (b-d) represent the electron distribution possibility. (a)Time profile of wave field. (b)Probability as a function of Energy E and time t: $Prob = P(\alpha_{eq0}, E_0, t; E)\Delta E$. (c)Probability as a function of equatorial pitch angle α_{eq} and time t: $Prob = P(\alpha_{eq0}, E_0, t; \alpha_{eq})\Delta\alpha_{eq}$. (d)Probability as a function of energy E and equatorial pitch angle α_{eq} at time $t = \tau = 4$ s.The asterisk represents the initial electrons probability distribution. (e-h):Four transport coefficients calculated with the same parameter settings as the model in (a-d) but with the energy range $E_0 \in (10^3, 10^7)eV$ and pitch angle range $\alpha_{eq} \in (60, 90)deg$. The colorbars in (e-h) represent the corresponding transport coefficient value. (e)The pitch angle diffusion coefficient $D_{\alpha\alpha}$ as a function of energy E and equatorial pitch angle α_{eq}. The three white solid lines denote the bounce resonance conditions for the first three harmonics, $\omega = \omega_b, \omega = 2\omega_b, \omega = 3\omega_b$. (f)The energy diffusion coefficient D_{EE} as a function of energy E and equatorial pitch angle α_{eq}. (g)The pitch angle advection coefficient A_α as a function of energy E and equatorial pitch angle α_{eq}. (h)The pitch angle advection coefficient A_E as a function of energy E and equatorial pitch angle α_{eq}.

ability function of α_{eq} or E is defined by the integral of the 2D probability function, and the explicit expressions are $P(\alpha_{eq0}, E_0, t; \alpha_{eq}) = \int P(\alpha_{eq0}, E_0, t; \alpha_{eq}, E)dE$, $P(\alpha_{eq0}, E_0, t; E) = \int P(\alpha_{eq0}, E_0, t; \alpha_{eq}, E)d\alpha_{eq}$. Figure 1(a-d) shows one example in that we initialize particles with a given $\alpha_{eq0} = 89.5$ deg and $E_0 = 300$ keV and then turn on the waves at $t = 0$, which is shown in Figure 1(a), and the time evolution of probability distribution of E and α_{eq} are shown in Figure 1(b) and (c), respectively. Figure 1 (d) shows an example of $P(\alpha_{eq0}, E_0, t; \alpha_{eq}, E)$ as a function of E and α_{eq} at time $t = \tau$, with the initial $\alpha_{eq0} = 89.5°$ and $E_0 = 300$ keV, which are represented by the asterisk.

As we can see, the particles are scattered from the initial energy 300 keV and initial equatorial pitch angle $\alpha_{eq} = 89.5$ deg. The transport process has two simultaneous effects, diffusion and advection. The former is the probability distribution broadening process in α_{eq} and E with time and the latter is the drifting of the peak probability of α_{eq} and E with time. These two transport coefficients are used to quantify the electron scattering effect. The diffusion coefficients of pitch angle and energy (Maldonado & Chen, 2018) are defined as:

$$D_{\alpha\alpha} = \frac{(\alpha_{eq} - [\alpha_{eq}])^2}{2t} \tag{8}$$

$$D_{EE} = \frac{(E - [E])^2}{2t} \tag{9}$$

The advection coefficients of pitch angle and energy are defined as:

$$A_{\alpha} = \frac{(\alpha_{eq} - [\alpha_{eq}])}{t} \tag{10}$$

$$A_{E} = \frac{(E - [E])}{t} \tag{11}$$

The operator [...] represents the ensemble average of α_{eq} or E over bounce phases and waves phases and its definition is

$$[Q] = \int\int d\alpha_{eq} dE \times Q \times P(\alpha_{eq0}, E_0, t; \alpha_{eq}, E) \tag{12}$$

Thus the transport coefficients can be described as a 2D function of (α_{eq0}, E_0) by calculating test particle simulation with different initial conditions. Figure 1 (e-f) present the four transport coefficients: the energy and pitch angle diffusion and advection coefficients at time $t = 4$s. One can clearly see that the diffusion coefficients $D_{\alpha\alpha}$ and D_{EE} reach their peaks around $\alpha_{eq0} = 85$ deg around 300 keV (Figure 1(e)(f)) while significant negative A_α and positive A_E appears near $\alpha_{eq0} = 90$ deg. One can expect that electrons with higher pitch angles have bigger transport coefficients since they have lower mirror latitude and will be accelerated with MS wave field more efficiently than those with lower pitch angles. Since we choose the wave center frequency $f_0 = f_{b0}$, no wonder the coefficients peaks locate around the energy around 300 keV, which satisfies the bounce resonant condition $\omega = \omega_b$.

One can clearly see multiple peaks in each coefficient in Figure 1(e-h) resulting from bounce resonance harmonics. In Figure 1(e), we plot the pitch angle diffusion coefficient together with bounce resonance harmonics conditions. We can see that the peaks in energy match with the harmonic bounce resonance condition $\omega = n\omega_b$, in which ω_b means the electron bounce angular frequency and n is a positive integer and represents the bounce harmonic order. We present the first three harmonics and find that different bounce harmonic resonances correspond to different peaks in the transport coefficients. Higher order harmonic resonances exist but the effect of fundamental resonance is much stronger. This is consistent with the conclusion in (Chen et al., 2015). Thus to achieve the most efficient bounce resonance transport effect to remove equatorially mirroring electrons away from oblique pitch angle, the low harmonic resonant condition should be satisfied.

We can compare the relative importance between diffusion and advection effect by calculating $\sqrt{D_{\alpha\alpha} \cdot t}$ and $|A_\alpha \cdot t|$. For example, to compare the two pitch angle transport effect of particles with 1 MeV and $\alpha_{eq0} = 90$ deg, $\sqrt{D_{\alpha\alpha} \cdot t} = \sqrt{0.02 \times 4}$ deg $\ll$ $|A_\alpha \cdot t| = |-0.30 \times 4|$ deg, which means that the advection dominates over diffusion in this case. One can also compare the relative importance between pitch angle diffusion and energy diffusion effect by calculating $D_{\alpha\alpha}$ and D_{EE}/E^2. Take the peak point in $D_{\alpha\alpha}$ and D_{EE} as an example. $D_{\alpha\alpha} \approx 1.2$ and $D_{EE}/E^2 \approx 2 \cdot 10^5/(3 \cdot 10^5)^2 \approx 10^{-6}$, thus we can get that the pitch angle diffusion is more important than energy diffusion. A similar comparison can be done for A_α and A_E by calculating $|A_\alpha|$ and $|A_E/E|$ and find the similar conclusion that pitch angle advection is more obvious than energy advection. This can be understood by using μ conservation. Since $\mu = E \sin \alpha_{eq}^2 / B_{eq}$ is conserved, $|\Delta\alpha_{eq}/\tan\alpha_{eq}| = |\Delta E/2E|$ and α_{eq} is near 90 deg, the relative change of α_{eq} is more significant than the relative change of ΔE. These peaks mean that the electrons are scattered most efficiently with corresponding energies and pitch angles under the given MS wave and background parameters. Considering that pitch angle transport is more important in this process, in the following parametric study section, pitch angle transport coefficients are more valuable to be investigated. The analytic diffusion coefficients for broadband waves have been obtained (Chen & Bortnik, 2020) but the advection coefficients remain little explored. And for $\alpha_{eq0} < 80$ deg, diffusion dominates over advection, while the response of nearly equatorially mirroring electrons is nonlinear with significant advection. Thus, we will use the A_α to represent the transport coefficients and their peaks to identify the most effective transport conditions of electrons energy and pitch angle in the following parametric study.

3 Parametric Study

In this section, we investigate the dependencies of the transport effect, which is represented by advection coefficient A_α, on the background and wave parameters, namely, root-mean-square wave magnetic amplitude B_{wrms}, center frequency f_0, frequency width δf, latitudinal distribution width λ_w, wave normal angle θ_0, L-shell value and plasma density N_0. Each time we will vary one parameter while keeping the others the same as the nominal case in Figure 1.

3.1 Wave Frequency Width δf

In Figure 2, we present the advection coefficient A_α together with the harmonic bounce resonance conditions. Figure 2(a-c) present the comparison of transport coefficient A_α with different wave frequency widths. When the frequency width δf is small, the wave can be seen as a monochromatic wave and different harmonic resonances effects are separate in energy. With δf increasing, the affected energy gets broader but the magnitude decreases, which means the bounce resonance transport effect will happen over a broad energy range but the effect itself decays. To understand why this happens, we need to use the simplified Equation (7). When the wave frequency width broadens, the frequency width for each discrete wave increases and the wave power spectrum density will decrease, the wave amplitude E_z^w and B_z^w will decrease, and the amplitude of the second term on the right hand side of Equation (7) will decrease, which will weaken the resonance effect.

3.2 Wave Center Frequency f_0

Figure 2(d-f) show the comparison of transport coefficient A_α with different wave center frequency f_0. Higher order resonance harmonics will dominate and play a significant role in electron transportation. The fundamental in (d) and first two harmonics in (e) disappear because the electron's bounce frequency has an upper limit due to relativistic effect and the resonant condition cannot be satisfied any more. By comparing

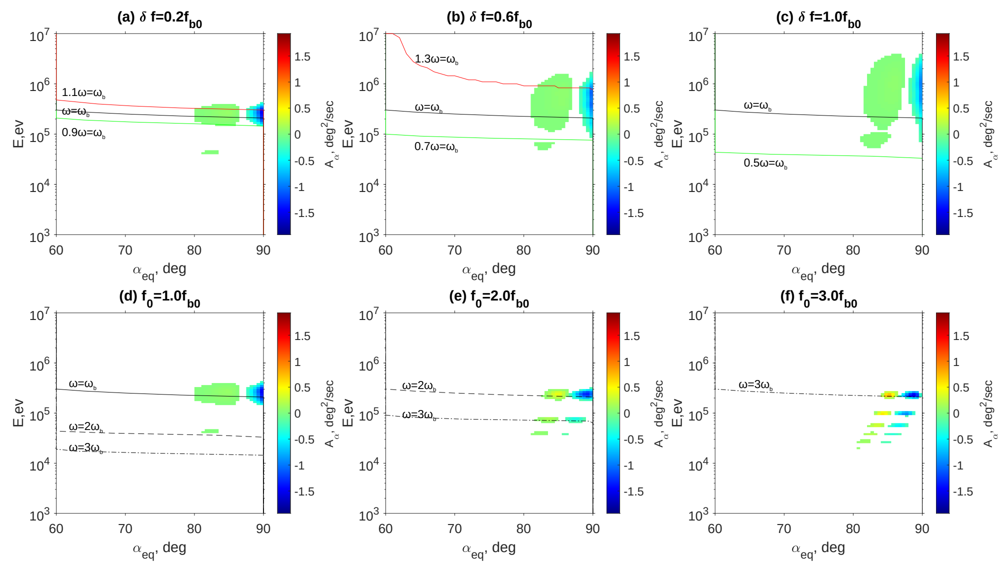

Figure 2. Transport coefficient A_α dependency on (a-c) frequency width and (d-f) center frequency. The red, black and green solid lines in (a-c) represent the wave frequency upper limit, center frequency and lower limit, respectively.The black solid, dashed, dot-dashed lines in (d-e) represent the bounce resonance conditions of $\omega = \omega_b, \omega = 2\omega_b, \omega = 3\omega_b$, respectively.

the peaks value in(d-f), one can see that the second(e) and the third(f) harmonic resonance transport effect in high wave frequency is comparable with the fundamental mode in low wave frequency. This is because when f_0 increases, the related $k_\perp$ decreases, $J_0(\beta)$ and $J_1(\beta)/\beta$ increase and will increase the amplitude of the second term on the right hand side of Equation (7).

3.3 Wave Latitudinal Distribution Width λ_w

Figure 3(a-c) shows the comparison of transport coefficient A_α with different latitudinal distribution width λ_w. One can see that A_α decreases with λ_w at first and then increases. Increasing λ_w enhances the wave power over a longer bouncing path and increases the transport but the transit time scattering (Bortnik & Thorne, 2010) may decrease as λ_w increases.

3.4 Wave Normal Angle θ_0

Figure 3(d-f) shows the comparison of transport coefficient A_α with different wave normal angle θ_0. One can easily find that with θ_0 increasing, A_α decreases. With increasing θ_0, β increases and k_z decreases and the amplitude of the second term on the right hand side of Equation (7) decreases, which will weaken the transport effect.

3.5 Root-Mean-Square Value of Wave Magnetic Field B_{wrms}

Figure 3(g-i) shows the comparison of transport coefficient A_α with different wave magnetic field amplitude B_{wrms}. Clearly, the transport coefficient A_α increases with B_{wrms} increasing. It is not surprising to get this result as E_z^w and B_z^w in the second term on

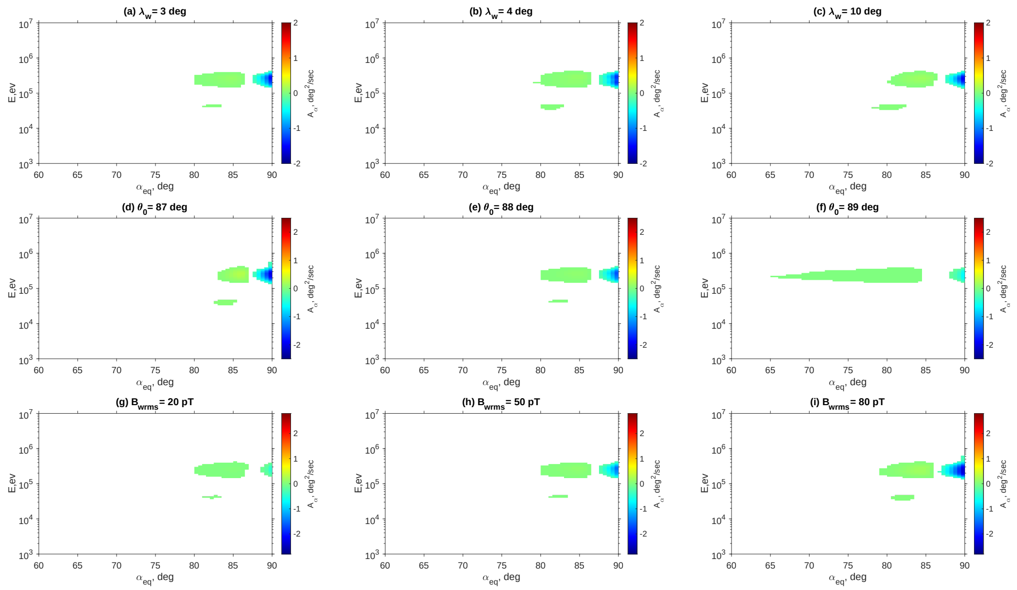

Figure 3. Transport coefficient A_α dependency on (a-c) wave latitudinal distribution width λ_w, (d-f) wave normal angle θ_0 and (g-i) root-mean-square of magnetic field amplitude B_{wrms}.

the right hand side of equation 7 will both increase. Furthermore, we can also find that the transport effect is linear with the wave amplitude since $dp_z/dt \propto E_z^W, B_z^w$, which has been verified but not shown here.

3.6 *L*-shell Value

Usually, L-shell value and plasma density N_0 are correlated since plasma density drops in order of magnitude at plasmapause and inside the plasmasphere (low L) N_0 is much bigger than that outside the plasmasphere (high L). However, the irregularities of the plasmasphere, like plumes, make it possible to have low L and low N_0, high L and high N_0. Therefore, we treat L and N_0 as independent variables. Figure 4 compares transport coefficient A_α with different L-shell value. We find that A_α increases when the L-shell value increases. Increasing L-shell value leads to higher μ since $\mu \propto L^3$, and will increase the amplitude of the second term on the right hand side of equation 7.

3.7 Plamsa Density N_0

We choose three typical values of N_0 to compare the transport coefficient A_α. $N_0 = 300, 100, 10cm^{-3}$ represent the plasma density inside the plasmasphere, near plasmapause and outside the plasmasphere, respectively. It is apparent that transport coefficient A_α increases with N_0 increasing. According to the properties of MS waves, $\omega/k_\perp \approx V_A(N_0), k_\perp/k_z = tan(\theta_0)$, where V_A is the Alfven velocity. Increasing N_0 results in smaller V_A and thus larger $k_\perp$ and k_z. Although larger $k_\perp$ will decrease J_0 and J_1/β, k_z's importance dominates and the amplitude of the second term on the right hand side of equation 7 increases.

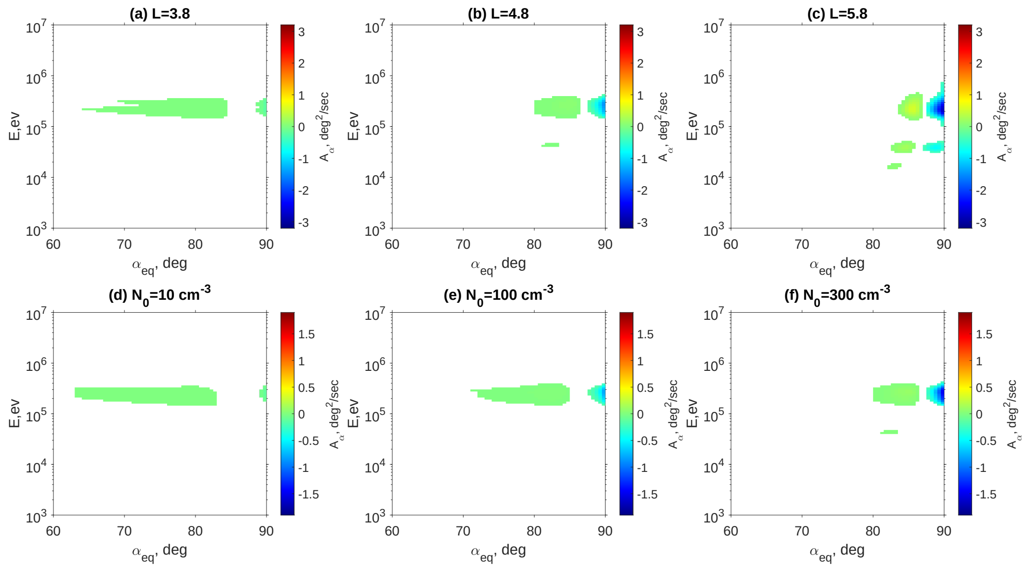

Figure 4. Transport coefficient A_α dependency on background parameters: (a-c) L-shell value and (d-f) plasma density N_0.

4 Conclusions and Discussion

In this study, we use test-particle simulation and investigate the equatorially mirroring electrons transport coefficients due to nonlinear bounce resonance with MS waves and its dependencies with wave field parameters (frequency width, center frequency, latitudinal width, wave normal angle and root-mean-square of wave amplitude) and background parameters (L-shell value and plasma density). Our principal conclusions are summarized as follows:

(1) Different bounce harmonic resonances correspond to different peaks in the transport coefficients. Higher order harmonic resonances exist but the effect of fundamental resonance is much stronger if present.

(2) With wave center frequency increasing, higher order harmonics start to dominate.

(3) The bounce resonance effect tends to increase with increasing latitudinal width, wave amplitude, L-shell value and plasma density, and decreasing wave normal angle and wave frequency width.

The diffusion or advection by bounce resonance with MS waves and parametric relationships in this study are expected to be incorporated into the radiation belt modeling. Previous modelings of electron diffusion pay main attention to gyroresonance with chorus or hiss waves, where the bounce motion is averaged and the bounce resonance effect is not considered (e.g. Xiao et al., 2009). The bounce resonance with MS waves should be taken into consideration (Chen et al., 2015; Tao et al., 2016) and our results of bounce diffusion can be implemented into the global simulation of electron diffusion. As to advection effect, the analytic expressions of advection coefficients remains unclear so far and the advection effect is usually not included in previous studies on electron transport. Zheng et al. (2021) proposed a numerical solver for Fokker-Planck equation of radiation belt, which contains the advection coefficients and provided a good framework to investigate the advection. It will be promising to use the adevetion coefficients calculated in this study as inputs of the model in Zheng et al. (2021) in the future.

The realistic MS waves usually have multiple equally spacing wave bands (Santolík et al., 2004; Min et al., 2018) while in this paper we consider only one wave frequency band in the wave model. Tao et al. (2013) investigated the amplitude modulation of a two-wave model for whistler mode waves and found the resonance overlap could result in different change of the electron pitch angle and energy from the ideal single-wave. An et al. (2014) established a two-wave model for electromagnetic ion cyclotron(EMIC) waves and adopted an oscillator dynamic system to understand the electron behavior. Compared with whistler mode waves and EMIC waves, MS waves have more obvious harmonic structures in frequency and the coherent interactions of electrons with MS waves needs to be investigated in the future.

Acknowledgments

References

An, X., Chen, L., Bortnik, J., & Thorne, R. M. (2014). An oscillator model representative of electron interactions with emic waves. *Journal of Geophysical Research: Space Physics*, *119*(3), 1951-1959. Retrieved from `https://agupubs.onlinelibrary.wiley.com/doi/abs/10.1002/2013JA019597` doi: https://doi.org/10.1002/2013JA019597

Blum, L., Artemyev, A., Agapitov, O., Mourenas, D., Boardsen, S., & Schiller, Q. (2019). Emic wave-driven bounce resonance scattering of energetic electrons in the inner magnetosphere. *Journal of Geophysical Research: Space Physics*, *124*(4), 2484-2496. Retrieved from `https://agupubs.onlinelibrary.wiley.com/doi/abs/10.1029/2018JA026427` doi: https://doi.org/10.1029/2018JA026427

Bortnik, J., & Thorne, R. M. (2010). Transit time scattering of energetic electrons due to equatorially confined magnetosonic waves. *Journal of Geophysical Research: Space Physics*, *115*(A7). Retrieved from `https://agupubs.onlinelibrary.wiley.com/doi/abs/10.1029/2010JA015283` doi: https://doi.org/10.1029/2010JA015283

Cao, X., Ni, B., Summers, D., Bortnik, J., Tao, X., Shprits, Y. Y., ... Wang, Q. (2017). Bounce resonance scattering of radiation belt electrons by h+ band emic waves. *Journal of Geophysical Research: Space Physics*, *122*(2), 1702-1713. Retrieved from `https://agupubs.onlinelibrary.wiley.com/doi/abs/10.1002/2016JA023607` doi: https://doi.org/10.1002/2016JA023607

Chen, L., & Bortnik, J. (2020). Chapter 4 - wave-particle interactions with coherent magnetosonic waves. In A. N. Jaynes & M. E. Usanova (Eds.), *The dynamic loss of earth's radiation belts* (p. 99-120). Elsevier. Retrieved from `https://www.sciencedirect.com/science/article/pii/B9780128133712000044` doi: https://doi.org/10.1016/B978-0-12-813371-2.00004-4

Chen, L., Maldonado, A., Bortnik, J., Thorne, R. M., Li, J., Dai, L., & Zhan, X. (2015). Nonlinear bounce resonances between magnetosonic waves and equatorially mirroring electrons. *Journal of Geophysical Research: Space Physics*, *120*(8), 6514-6527. Retrieved from `https://agupubs.onlinelibrary.wiley.com/doi/abs/10.1002/2015JA021174` doi: https://doi.org/10.1002/2015JA021174

Chen, L., & Thorne, R. M. (2012). Perpendicular propagation of magnetosonic waves. *Geophysical Research Letters*, *39*(14). Retrieved from `https://agupubs.onlinelibrary.wiley.com/doi/abs/10.1029/2012GL052485` doi: https://doi.org/10.1029/2012GL052485

Chen, L., Thorne, R. M., Jordanova, V. K., Thomsen, M. F., & Horne, R. B. (2011). Magnetosonic wave instability analysis for proton ring distributions observed by the lanl magnetospheric plasma analyzer. *Journal of Geophysical Research: Space Physics*, *116*(A3). Retrieved from https://agupubs.onlinelibrary.wiley.com/doi/abs/10.1029/2010JA016068 doi: https://doi.org/10.1029/2010JA016068

Gary, S. P., Liu, K., Winske, D., & Denton, R. E. (2010). Ion bernstein instability in the terrestrial magnetosphere: Linear dispersion theory. *Journal of Geophysical Research: Space Physics*, *115*(A12). Retrieved from https://agupubs.onlinelibrary.wiley.com/doi/abs/10.1029/2010JA015965 doi: https://doi.org/10.1029/2010JA015965

Gurnett, D. A. (1976). Plasma wave interactions with energetic ions near the magnetic equator. *Journal of Geophysical Research (1896-1977)*, *81*(16), 2765-2770. Retrieved from https://agupubs.onlinelibrary.wiley.com/doi/abs/10.1029/JA081i016p02765 doi: https://doi.org/10.1029/JA081i016p02765

Hanzelka, M., Němec, F., Santolík, O., & Parrot, M. (2022). Statistical analysis of wave propagation properties of equatorial noise observed at low altitudes. *Journal of Geophysical Research: Space Physics*, *127*(7), e2022JA030416. Retrieved from https://agupubs.onlinelibrary.wiley.com/doi/abs/10.1029/2022JA030416 (e2022JA030416 2022JA030416) doi: https://doi.org/10.1029/2022JA030416

Li, X., & Tao, X. (2018). Validation and analysis of bounce resonance diffusion coefficients. *Journal of Geophysical Research: Space Physics*, *123*(1), 104-113. Retrieved from https://agupubs.onlinelibrary.wiley.com/doi/abs/10.1002/2017JA024506 doi: https://doi.org/10.1002/2017JA024506

Li, X., Tao, X., Lu, Q., & Dai, L. (2015). Bounce resonance diffusion coefficients for spatially confined waves. *Geophysical Research Letters*, *42*(22), 9591-9599. Retrieved from https://agupubs.onlinelibrary.wiley.com/doi/abs/10.1002/2015GL066324 doi: https://doi.org/10.1002/2015GL066324

Liu, K., Gary, S. P., & Winske, D. (2011). Excitation of magnetosonic waves in the terrestrial magnetosphere: Particle-in-cell simulations. *Journal of Geophysical Research: Space Physics*, *116*(A7). Retrieved from https://agupubs.onlinelibrary.wiley.com/doi/abs/10.1029/2010JA016372 doi: https://doi.org/10.1029/2010JA016372

Liu, Z.-Y., Zong, Q.-G., Zhou, X.-Z., Zhu, Y.-F., & Gu, S.-J. (2020). Pitch angle structures of ring current ions induced by evolving poloidal ultra-low frequency waves. *Geophysical Research Letters*, *47*(4), e2020GL087203. Retrieved from https://agupubs.onlinelibrary.wiley.com/doi/abs/10.1029/2020GL087203 (e2020GL087203 10.1029/2020GL087203) doi: https://doi.org/10.1029/2020GL087203

Ma, Q., Li, W., Thorne, R. M., & Angelopoulos, V. (2013). Global distribution of equatorial magnetosonic waves observed by themis. *Geophysical Research Letters*, *40*(10), 1895-1901. Retrieved from https://agupubs.onlinelibrary.wiley.com/doi/abs/10.1002/grl.50434 doi: https://doi.org/10.1002/grl.50434

Maldonado, A. A., & Chen, L. (2018). On the diffusion rates of electron bounce resonant scattering by magnetosonic waves. *Geophysical Research Letters*, *45*(8), 3328-3337. Retrieved from https://agupubs.onlinelibrary.wiley.com/doi/abs/10.1002/2017GL076560 doi: https://doi.org/10.1002/2017GL076560

Maldonado, A. A., Chen, L., Claudepierre, S. G., Bortnik, J., Thorne, R. M., & Spence, H. (2016). Electron butterfly distribution modulation by magnetosonic waves. *Geophysical Research Letters*, *43*(7), 3051-3059. Retrieved from https://agupubs.onlinelibrary.wiley.com/doi/abs/10.1002/2016GL068161 doi: https://doi.org/10.1002/2016GL068161

Min, K., Liu, K., Wang, X., Chen, L., & Denton, R. E. (2018). Fast magnetosonic waves observed by van allen probes: Testing local wave excitation mechanism. *Journal of Geophysical Research: Space Physics*, *123*(1), 497-512. Retrieved from https://agupubs.onlinelibrary.wiley.com/doi/abs/10.1002/2017JA024867 doi: https://doi.org/10.1002/2017JA024867

Roberts, C. S., & Schulz, M. (1968). Bounce resonant scattering of particles trapped in the earth's magnetic field. *Journal of Geophysical Research (1896-1977)*, *73*(23), 7361-7376. Retrieved from https://agupubs.onlinelibrary.wiley.com/doi/abs/10.1029/JA073i023p07361 doi: https://doi.org/10.1029/JA073i023p07361

Russell, C. T., Holzer, R. E., & Smith, E. J. (1969). Ogo 3 observations of elf noise in the magnetosphere: 1. spatial extent and frequency of occurrence. *Journal of Geophysical Research (1896-1977)*, *74*(3), 755-777. Retrieved from https://agupubs.onlinelibrary.wiley.com/doi/abs/10.1029/JA074i003p00755 doi: https://doi.org/10.1029/JA074i003p00755

Santolík, O., Němec, F., Gereová, K., Macúšová, E., de Conchy, Y., & Cornilleau-Wehrlin, N. (2004). Systematic analysis of equatorial noise below the lower hybrid frequency. *Annales Geophysicae*, *22*(7), 2587–2595. Retrieved from https://angeo.copernicus.org/articles/22/2587/2004/ doi: 10.5194/angeo-22-2587-2004

Shprits, Y. Y. (2009). Potential waves for pitch-angle scattering of near-equatorially mirroring energetic electrons due to the violation of the second adiabatic invariant. *Geophysical Research Letters*, *36*(12). Retrieved from https://agupubs.onlinelibrary.wiley.com/doi/abs/10.1029/2009GL038322 doi: https://doi.org/10.1029/2009GL038322

Tao, X., & Bortnik, J. (2010). Nonlinear interactions between relativistic radiation belt electrons and oblique whistler mode waves. *Nonlinear Processes in Geophysics*, *17*(5), 599–604. Retrieved from https://npg.copernicus.org/articles/17/599/2010/ doi: 10.5194/npg-17-599-2010

Tao, X., Bortnik, J., Albert, J., Thorne, R., & Li, W. (2013). The importance of amplitude modulation in nonlinear interactions between electrons and large amplitude whistler waves. *Journal of Atmospheric and Solar-Terrestrial Physics*, *99*, 67-72. Retrieved from https://www.sciencedirect.com/science/article/pii/S1364682612001411 (Dynamics of the Complex Geospace System) doi: https://doi.org/10.1016/j.jastp.2012.05.012

Tao, X., Zhang, L., Wang, C., Li, X., Albert, J. M., & Chan, A. A. (2016). An efficient and positivity-preserving layer method for modeling radiation belt diffusion processes. *Journal of Geophysical Research: Space Physics*, *121*(1), 305-320. Retrieved from https://agupubs.onlinelibrary.wiley.com/doi/abs/10.1002/2015JA022064 doi: https://doi.org/10.1002/2015JA022064

Tsurutani, B. T., Falkowski, B. J., Pickett, J. S., Verkhoglyadova, O. P., Santolik, O., & Lakhina, G. S. (2014). Extremely intense elf magnetosonic waves: A survey of polar observations. *Journal of Geophysical Research: Space Physics*, *119*(2), 964-977. Retrieved from https://agupubs.onlinelibrary.wiley.com/doi/abs/10.1002/2013JA019284 doi: https://doi.org/10.1002/2013JA019284

Xiao, F., Su, Z., Zheng, H., & Wang, S. (2009). Modeling of outer radiation belt electrons by multidimensional diffusion process. *Journal of Geophysical Research: Space Physics*, *114*(A3). Retrieved from https://agupubs.onlinelibrary.wiley.com/doi/abs/10.1029/2008JA013580 doi: https://doi.org/10.1029/2008JA013580

Zheng, L., Chen, L., Chan, A. A., Wang, P., Xia, Z., & Liu, X. (2021). Uber v1.0: a universal kinetic equation solver for radiation belts. *Geoscientific Model Development*, *14*(9), 5825–5842. Retrieved from https://gmd.copernicus.org/articles/14/5825/2021/ doi: 10.5194/gmd-14-5825-2021

Zhu, Y.-F., Gu, S.-J., Zhou, X.-Z., Zong, Q.-G., Ren, J., Sun, X.-R., … Rankin, R. (2020). Drift-bounce resonance between charged particles and ultralow frequency waves: Theory and observations. *Journal of Geophysical Research: Space Physics*, *125*(1), e2019JA027067. Retrieved from `https://agupubs.onlinelibrary.wiley.com/doi/abs/10.1029/2019JA027067` (e2019JA027067 10.1029/2019JA027067) doi: https://doi.org/10.1029/2019JA027067